CARBON INJECTION INTO ELECTRIC ARC FURNACE SLAGS

CARBON INJECTION INTO ELECTRIC ARC FURNACE SLAGS

By

TAI XI ZHU, B.Eng.

A Thesis

Submitted to the School of Graduate Studies

In Partial Fulfillment of the Requirements

For the Degree

Master of Applied Science

McMaster University

MASTER OF APPLIED SCIENCE (2011) McMaster University

(Materials Science and Engineering) Hamilton, Ontario, Canada

TITLE: Carbon Injection into Electric Arc Furnace Slags

AUTHOR: Tai Xi Zhu, B. Eng. (McMaster University, Canada)

SUPERVISOR: Dr. Kenneth S. Coley

NUMBER OF PAGES: ix, 94

ABSTRACT

Recent experiment in our laboratory demonstrates that an increase in slag foaming with carbon injection rate is limited by slag volume. The current work has identified a relationship between foam height, carbon injection rate and slag volumes, which predicts the critical injection rate above which foaming become inefficient. The prediction of critical injection rate employs an extension of understanding mechanism of bubble movement in the foam by estimating average/steady-state bubble size and wall thickness. The carbon gasification model developed in our laboratory by King et al., which has been extended to include greater consideration of gas bubble bursting when to predict bubble size, and further improvement for calculating how fast bubble can burst instantaneously in carbon-gas-slag halo system, has found that has important influence on the predicting foaming parameters in King's model, which is crucial task for continuous development in future.

ACKNOLEDGEMENTS

I am sincerely grateful to my supervisor, Dr. K.S. Coley, for his patient guidance and countless encouragement. I am very appreciative for the learning opportunities and financial support I was given whilst studying under his direction. His invaluable advice has played a key role in accomplishing this work.

I would like to express my sincere gratitude to Dr. G.A. Irons, for his mentoring advice and assistance. I wish to thank Mr. Owen Kelly, John Thompson, Dr. Kumar Krishnaposharody and Dr. F.Z. Ji, for their tireless help in my experiments.

I would like to thank the McMaster Steel Research Center and the Natural Sciences and Engineering Research Council of Canada, for their generous financial support of my graduate studies.

Finally, I owe priceless to my parents, Yuyan Zhu and Hong Gao, for all their support thorough my life.

Table of Contents

LIST OF FIGURES

LIST OF TABLES

Chapter 1: Introduction

Since 1907, when the first commercial Electric Arc Furnace (EAF) was built for steelmaking, the development route has gone through continuous evolution and innovation. The modern EAF process employs many of the following: a pre-heating system, a single-bucket operation, a twin-shell furnace, co-axial and supersonic lances for oxygen, carbon injection and natural gas injection. These technologies have not only greatly improved energy consumption (energy per ton of steel produced) but have also contributed to environmental sustainability by recycling raw material - scrap.

In the EAF process, carbon, in the form of coke or coal, is injected into molten slag in the late stages of scrap melting. This carbon reacts with iron oxide in the slag, creating gas, which causes slag foaming. The kinetics of oxidization of carbonaceous materials have been extensively studied by Turkdogan et al., 1968; Turkdogan and Vinters, 1969 and 1970; Tien and Turkdogan, 1970; Story et al., 1998; Fruehan et al., 2000; Story and Fruehan, 2000; Warczok and Utigard, 2000. Such oxidization processes in slag have also been researched by Mori et al., 1996; Li et al., 2000; Li and Ratchev; 2005 and 2006, Ji et al., 2002, 2003, 2004 and 2005; Barati and Coley, 2006; King 2009. Studies in slag foaming and foaming models conducted by Ito and Fruehan, 1989; Jiang and Fruehan, 1991; Zhang, 1992; Ogawa et al., 1993; Zhang and Fruehan, 1995; Ozturk and Fruehan, 1995; Jung and Fruehan, 2000; Lahiri and Seetharaman, 2002; Lotun and Pilon, 2005, King, 2009, Corbari and Fruehan, 2009; have provided important knowledge on how

chemical and physical properties of slag affect foaming, and the stability of bubbles. Arguably the most impactful work in this area was the pioneering research by Fruehan and co-workers who developed the foaming index concept. All of the issues introduced above, will be discussed in-depth in Chapter 2.

Chapter 2: Literature Review

2.1 Carbon Injection into EAF slags

In modern EAF steelmaking, carbon in the form of coke, char or coal, is injected into the furnace and reacts with slags (FeO/Fe_2O_3, CaO, MgO etc.) and post-combustion gas (CO_2). Those reactions produce gas, which causes the slag to foam. This foam can protect the refractory furnace lining, decrease heat loss, lessen electrode consumption and abate noise during the process. The main reactions include:

$$C(s) + O(slag) = CO\ (g) \quad (2.1)$$

$$FeO/\ Fe_2O_3 + CO(g) = Fe(l)/FeO + CO_2 \quad (2.2)$$

$$CO_2(g) + C(s) = 2CO(g) \quad (2.3)$$

Whilst carbon in the form of graphite is often used in laboratory research, coal or coke is the major carbon source used in the steel industry because of its low cost and multiple applications. Volatiles in coal may have an effect in the gasification reaction. The major volatile constituents include water, as well as methane and hydrogen which oxidize to produce water vapor. Water vapor can react with carbon as follows:

$$H_2O(g) + C(s) = CO\ (g) + H_2 \quad (2.4)$$

Nagasaka and Fruehan (1994) researched the kinetics of the reaction of H_2O with injected carbon and concluded that H_2O reacts at a faster rate than CO_2. Story and Fruehan (1989,

1993, and 2000) indicated that 3-4 wt% hydrogen in coal can create up to 30 vol. pct of H_2 and H_2O in the off-gas.

2.2 EAF Slags and Foam

The oxide components (slag) in EAF steelmaking are normally used to protect the furnace refractory and supply oxygen (O) for the chemical reaction with carbon. The slag composition controls chemical properties, such as basicity, as well as physical properties such as surface tension and viscosity. In the metals industry mixtures of oxides, CaO, MgO, MnO, Al_2O_3 SiO_2, P_2O_5 etc, are called slags and typically form in the EAF by a combination of oxidation of the metal and the addition of fluxes. In studies of slag foaming and slag properties, researchers have mainly focused on CaO-SiO_2-FeOx slag (Fruehan and Ito 1989, Barati and Coley 2005, 2006, 2009), or CaO- Al_2O_3-SiO_2-FeO slag (Fruehan et al. 1995, Li and Ratchev 2002) or occasionally more complex mixtures (Morales et al. 2002) together with C-CO-CO_2 mixture.

2.2.1 Critical Carbon Injection Rate

Most recently, King (2009) plotted the relationship between slag foam height and superficial gas velocity, as is shown in Figure 2.1. From the work of Freuhan and co-

workers on the foaming index, one would expect a linear relationship between superficial gas velocity and foam height. However from Figure 2.1, in the case of the lower temperature range data, there is a departure from the initial linear relationship at high superficial gas velocities. This observation led to interest in the present work regarding whether there is a critical foam height, beyond which carbon injection will lose its efficiency, and whether this critical foam height is affected by slag volume.

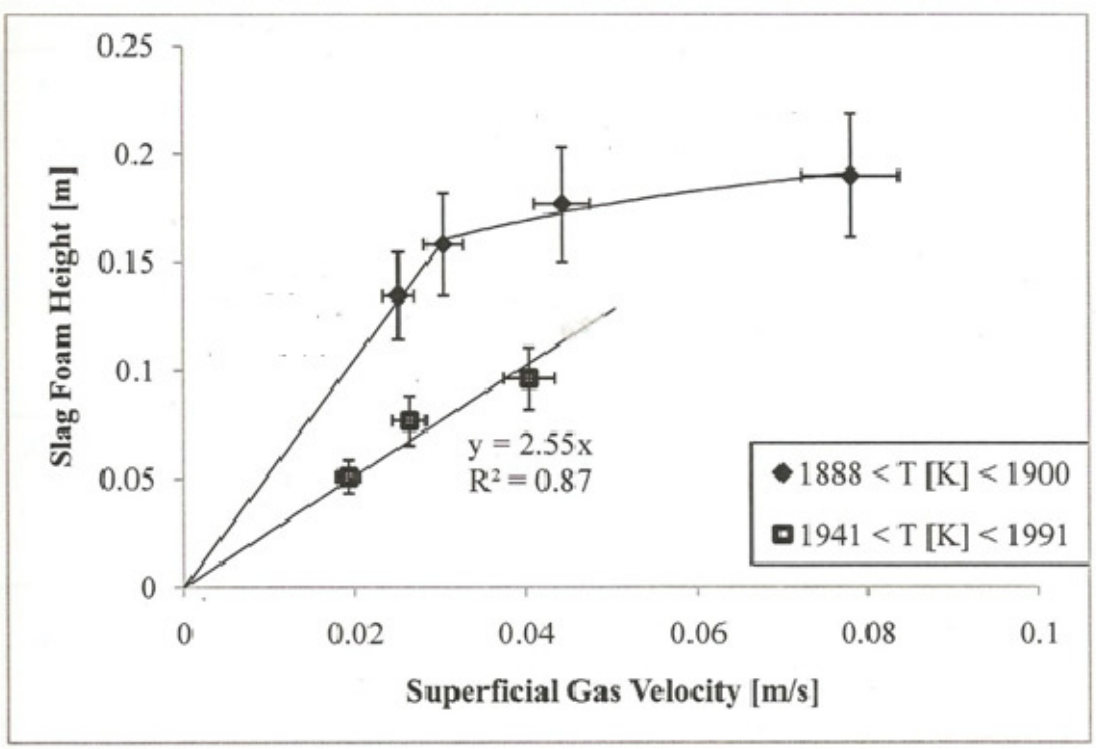

Figure 2. 1 Slag foam height vs. superficial gas velocity (King, 2009)

2.2.2 Foam Index

The Foam index Σ is an intermediate parameter that helps us to understand foaming in the EAF. It was first defined by Ito and Fruehan (1989) in the units of time (s), and represents average time for a bubble to travel through foam layers. When foam performance is ideal, the foam index can be expressed as the foam or bubble life time. The ideal condition exists when bubbles burst immediately upon reaching the upper surface of the foam. In this case, foam and liquid are in steady state during bubble movement, and all bubbles in the foam are perfectly spherical. Therefore, calculations based on Bikerman (1973) can be employed to express the foam index as follows:

$$\Sigma = \frac{\Delta h}{Q_g / A} = \frac{\Delta h}{\Delta V_g^s} \qquad (2.5)$$

A – furnace section area

Δh - change of foam height

Q_g -gas flow rate (cm^3 / s)

ΔV_g^s - superficial gas velocity (cm/s)

And foam life time was defined as follows:

$$\tau = -\frac{t}{\ln(\frac{h}{h_0})} \qquad (2.6)$$

t is the time foam height changed from h_0 to h.

Superficial gas velocity, defined as the volumetric flow rate of gas divided by the cross-sectional area (Gou et al., 1996) in the units of [m s^{-1}], is used in slag foaming to describe the gas generation rate. The calculation of superficial gas velocity in carbon injection experiments is shown below.

$$V_g^s = \frac{Q_g}{A_c} = \frac{(\frac{T}{273})(\frac{22.414}{1000})Q_c}{\frac{\pi}{4}d_{cru}^2} \tag{2.7}$$

Where Q_g is carbon gasification rate obtained from experiment in unit of [mol s^{-1}], T is gas temperature in unit of [K], d_{cru} is the diameter of the crucible in unit of [m], and V^s_g is superficial gas velocity in unit of [m s^{-1}]. The slag foam height was obtained directly from experimental measurements.

Fruehan and Ito (1989) conducted experiments which showed the foam height to be proportional to gas flow rate. The foam index is independent of crucible diameter and the foam index is constant when gas flow rate reaches steady state. In CaO-SiO_2-FeO slags at 1573K, the foam index was found to be inversely proportional to basicity. In 35wt%CaO-35wt%SiO_2-30wt%FeO slags, rising temperature destabilized the foam or depressed the

height of foam. Additives also have an influence on the foam index by altering physical properties such as viscosity or surface tension.

Fruehan and Ito researched the CaO-SiO_2-FeO (Al_2O_3) system in the temperature range 1073K to 1273K and determined the relationship between the foam index and slag properties such as density, surface tension and viscosity. By dimensional analysis of experimental data they proposed the following relationship:

$$\Sigma = 5.7 \times 10^2 \frac{\mu}{\sqrt{\sigma\rho}} \qquad (2.8)$$

Where μ is slag viscosity, σ is slag surface tension, ρ is slag density. Fruehan and Ito (1989) stated that this model is based on certain assumptions such as isothermal conditions, steady state flow, no effect from bubble size and uniform structure of slag foam. Because their experimental results were obtained on a laboratory scale, the complexity was much less than in an industrial EAF or bath smelting process. They also suggested that FeO has a strong influence on the slag foam height and foam index for slags with CaO/SiO_2 =3 at 1873K. Their experimental results showed that foam height reaches its highest level when FeO=25 to 30 wt%, as shown in Figure 2.2.

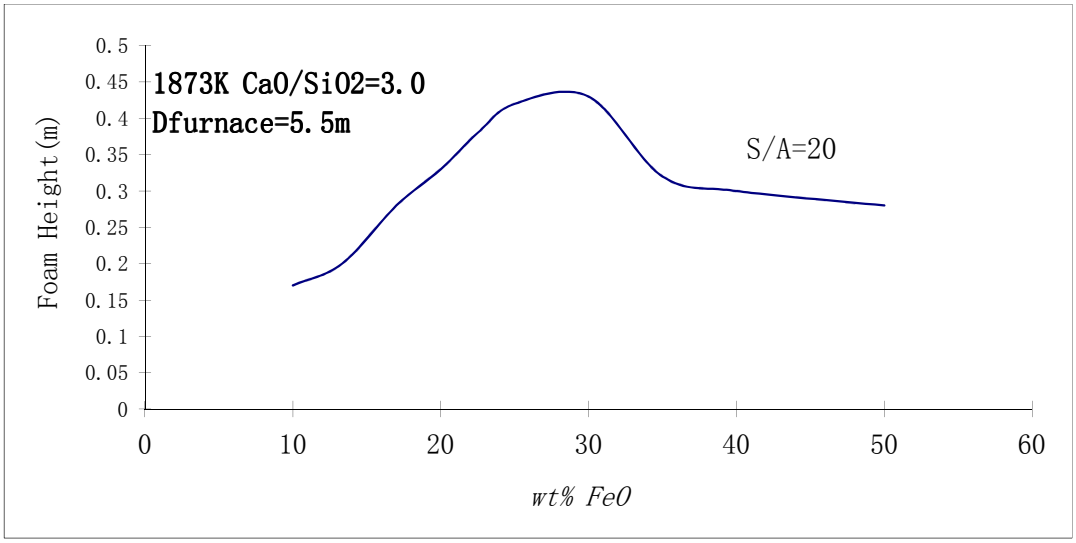

Figure 2. 2 Foam height vs. FeO concentration for EAF slag (Fruehan et al. 1989)

Although Ito and Fruehan (1989) introduced the concept of foam index and its mathematical representation, it has since been developed further to extend its range of application. Jiang and Fruehan (1991) modified the foam index for CaO-SiO_2-Al_2O_3-FeO slag, for FeO less than 15 wt% and by employing more accurate slag viscosity and surface tension data, they developed a revised expression for foam index, given in Equation 2.9

$$\Sigma = 115 \frac{\mu}{\sqrt{\sigma \rho}} \qquad (2.9)$$

Zhang and Fruehan (1995) discussed the foam index and conducted experiments for CaO-SiO_2-Al_2O_3-FeO slag at 1773K, in the composition range FeO 5 to 15 wt%., and CaO/SiO_2 = 1. Meanwhile Zhang used multi-orifice gas injection into the liquid slag which was found to increase the foam index compared to single-orifice injection. The sulfur content of slag appears to decrease the foam index. Bikerman (1973), suggested that foam mostly forms with either a beer-like or soap-like structure. Beer-like foam consists of small spherical bubbles in the liquid and it is mainly stable. Soap-like foams have a polyhedral structure and large bubbles, and are frequently unstable with thin films of liquid between the bubbles. Therefore, bubble size also has an influence on the foam index. Large average bubble size normally favors bubble bursting, and results in a short foam life or decreased foam index. Based on their observations of these effects, Zhang and Fruehan (1995) correlated the foam index with bubble size, producing the following equation:

$$\Sigma = 115 \frac{\mu^{1.2}}{\sigma^{0.2} \rho D_b^{0.9}} \qquad (2.10)$$

where D_b is average bubble diameter (m)

This equation was based on experiments using multi-orifice injection which has a closer relationship with coke injection, because of the multi-point bubble generation. By observing the effect of coke particles floating on the slag surface, Zhang and Fruehan (1995) discovered that carbonaceous material suppressed slag foaming. In comparison, wettable particles or materials, such as iron ore or alumina, did not suppress foaming.

They proposed that carbonaceous particles decrease foam height because there is a difference between the physical contact angle and equilibrium contact angle, which, during the movement of carbonaceous particles in the foam, causes bubbles to rupture.

Lotun and Pilon (2005) summarized foam index models below for CaO-SiO_2-FeO-MgO-Al_2O_3 slags:

Skupien and Gaskel (2000) at 1573 to 1708K

$$\Sigma = 100 \frac{\mu^{0.54}}{\rho^{0.39}\sigma^{0.15}} \tag{2.11}$$

Ghag et al. (1998) introduced effective elasticity of bubble film E_{eff} and modified foam index as:

$$\Sigma = 5\times10^{5} \frac{\mu E_{eff}}{(\rho g D)^{2}} \tag{2.12}$$

Zhu and Du (2000) predicted foam index on high viscosity liquid as given below:

$$\Sigma = 2905 \frac{\sigma[\mu(j - j_m)]^{0.8}}{(\rho g)^{1.8} r^{2.6}} \tag{2.13}$$

j –superficial gas velocity

j_m - is minimum superficial gas velocity to create foaming

r –average bubble radius

Luton and Pilon analyzed different foam indices using their own experimental data and applied Buckingham's Pi theorem to develop a relationship among foam height, bubble size and slag properties:

$$\frac{h}{r} = 2617 \frac{\mu^{0.73} j_r^{0.79} \sigma^{1.01}}{\rho^{1.74} g^{1.77} r^{3.51}} \tag{2.14}$$

h- foam height

r- average bubble radius

j_r - reduced superficial gas velocity

Luton then discussed surface tension as being proportional to bubble radius, and emphasized that foaming models were founded on steady state and idealized slag which is not necessarily the case on an industrial scale.

Corbari et al. (2009), employing Fruehan's work, suggested that research to date and foam indices do not represent real foaming in an EAF, because slag composition is not stable and multiple reactions disturb foam properties. In addition, they suggested that the foam index was further limited in predicting foam height in real industrial furnaces since carbonaceous materials (coal, char, etc.) may suppress foaming. Corbari also discussed the effect of FeO content on foam height and on foam index at 1823 K. This work showed FeO content had a more significant effect on foam height than gas generation when FeO

was in the range 15 to 25 wt%. The experimental comparisons are given by the following figure and table.

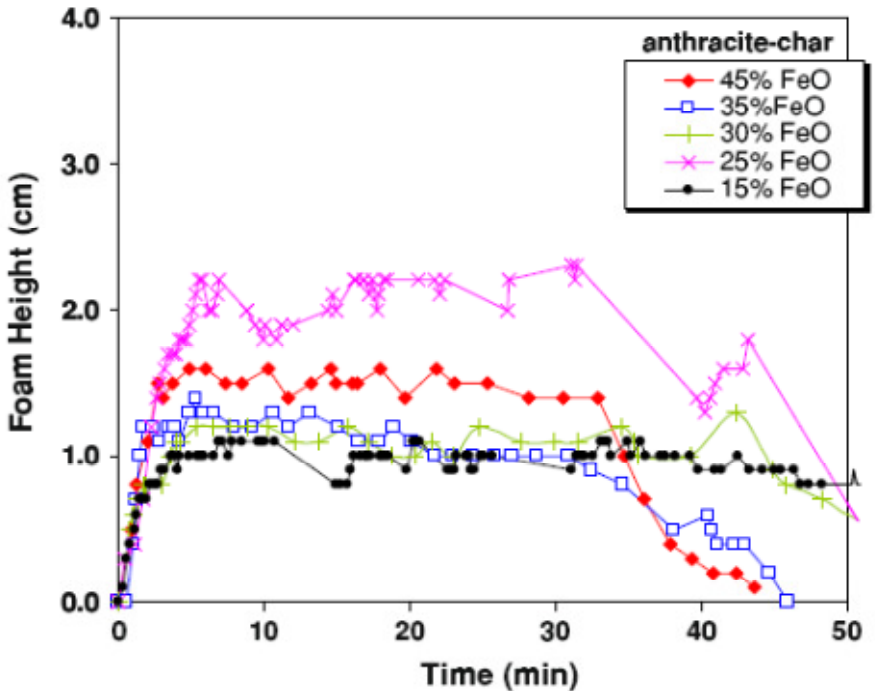

.

Figure 2. 3 Foam height vs. time for various FeO contents in Char additive slag at 1823 K (Corbari et al. 2009)

Table 2. 1 Relative Foam Indices for various FeO content at 1823 K

FeO wt%	$\frac{\Sigma}{\Sigma_{15wt\%FeO}}$
15	**1.00**
25	**0.71**
35	**0.51**
45	**0.41**

2.2.3 Dynamic Foam Index

Morales et al. (2001) first introduced the concept of dynamic foaming index. The major purpose of this research was to develop a mathematical model to predict foaming for an industrial scale EAF, and this model was evaluated for injection of oxygen and carbon into slag. Morales, Conejo and Rodriguez (2001) mentioned that this model offers a relatively accurate prediction of foam behavior in the EAF, but certain assumptions should be considered:

1) Metal-slag interfacial area is 1.5 times that of the static interface
2) The liquid steel contains only Fe and C

3) Carbon is injected at a 60 degree angle to the melt surface using 48mm diameter lance
4) Off-gas is mainly CO
5) Bath temperature is calculated by:

Tb= 1908-88(wt% C) [K] (2.15)

The foaming ratio, f, was defined as the ratio of volume change of both foam and slag to that of volume change of slag. Their equations are given as 2.16-2.18.

$$f = \frac{Q_g^{sl}}{Q_{sl}} \tag{2.16}$$

$$Q_g^{sl} = \frac{dV_{co}}{dt} + \frac{1}{[2460 + 18(\text{wt\%FeO})]} \frac{dW_{sl}}{dt} \tag{2.17}$$

$$Q_{sl} = \frac{1}{[2460 + 18(\text{wt\%FeO})]} \frac{dW_{sl}}{dt} \tag{2.18}$$

V_{co} - volume of CO produced

W_{sl} - mass of molten slag

Therefore, when f=1, $\frac{dV_{co}}{dt}$ is about zero so that there is no further CO produced and foaming is not set up or rising. In addition, dynamic foam index was represented by the equation below:

$$\Sigma_b = f\Sigma \quad (2.19)$$

Σ_b - dynamic foam index

Σ - static foam index

The mechanism in Dynamic Foam index (DFI) assumes that carbon is injected into slag and first reacts at the slag, and generates a bubble where CO_2 reacts with the slag to form CO. The reactions are shown below:

$$FeO + CO = [Fe] + CO_2 \quad (2.20)$$

$$CO_2 + C = 2\ CO \quad (2.21)$$

The second reaction is usually the rate determining step assuming that gas phase diffusion is fast.

Morales then applied this model to an EAF at Ispat Mexicana (IMEXSA), Lazaro Cardenas steelworks. The furnace had a 220 ton capacity, a 711 mm diameter electrode, a 125 MVA transformer and the feedstock was direct reduced iron, DRI. The industrial practice included injection of both carbon particles (10 to 120kg C/min) and oxygen. The model was used to calculate the foam height, which was then used to correct the

calculation of the DRI melting rate. The corrected DRI melting rate is given in equation 2.22, where the %metallisation is defined as the ratio of metallic iron to total iron in the product.

$$\frac{dW_{DRI}}{dt} = -226403.57 + 5016.66(\%metallisation) - 27.83(\%metallisation)^2 \qquad (2.22)$$

Arc distortion was used by these workers as a measure of foaming and Figure 2.4 shows excellent agreement between the reciprocal of arc distortion and the DFI over the course of a single heat.

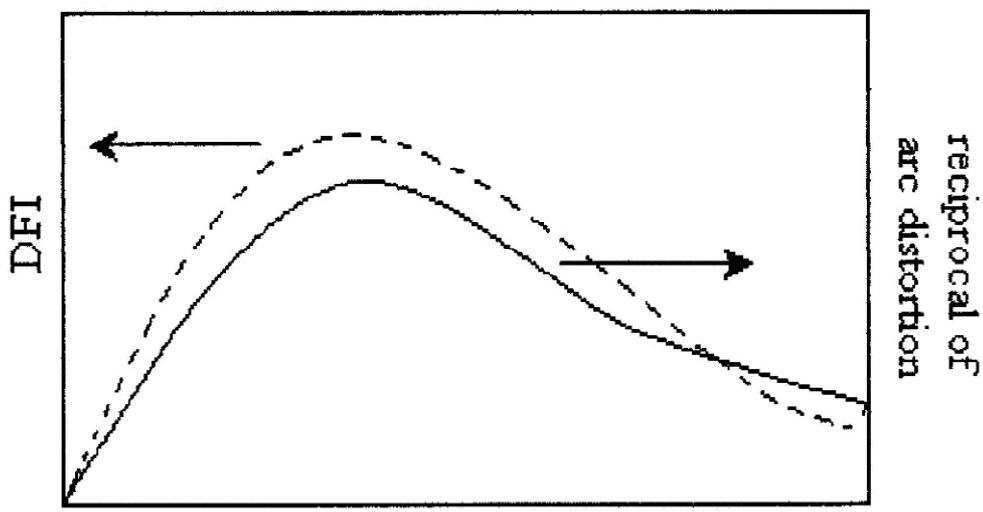

Figure 2. 4 Relationship between reciprocal arc distortion and Dynamic Foam Index (Morales et al. 2001)

2.2.4 Carbon-Slag Reaction Model

In developing a fundamental model for the kinetics carbon injection into slag and slag foaming, King (2009) reviewed work by Freuhan et al. (1989,1991,1995,2000,2005) on foam index, improved the kinetic model of Ji et al (2002, 2005, 2006) and applied the work of Turkdogan and Vinters (1970) on carbon-gas reaction kinetics. A physical picture of King's reaction model is shown in Figure 2.5

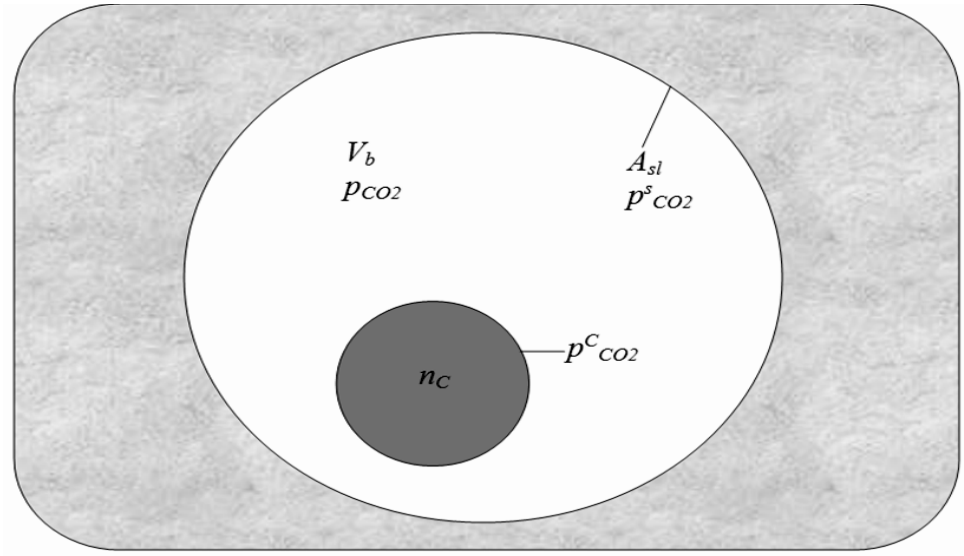

Figure 2. 5 Diagram of carbon-gas-slag system (King, 2009)

King developed a model to predict instantaneous carbon content in the slag and connected the output to predict other foaming parameters, such as average bubble size and carbon gasification rate. Their results showed reasonable agreement with experimental data but did not fit perfectly.

The suggested assumptions for King's model are as follows:

1) Carbon-slag reaction proceeds by complete internal burning.
2) The solid carbon, gas and slag are each uniform in temperature and composition.
3) Carbon reactivity is constant.
4) Gas phase only includes CO and CO_2
5) Total gas pressure in furnace is 1 atm.
6) Foam primarily consists of only spherical bubble.
7) The volume of solid carbon are negligible, because King stated that the bubble grows quickly and at 0.5 s is predicted to be over 4.5 time the diameter, and thus more than 95 times the volume, of the carbon particle.
8) Carbon injection is steady.
9) Injected carbon particles have same initial density and size.

The evolution of the model started with a single carbon particle reacting with slag and gas, the combined reaction is:

$$C(s) + O(slag) = CO(g) \qquad (2.23)$$

According to the above equation, the rate of C and O consumption is equal negative rate of CO consumption. This can be expressed as follows:

$$\frac{dn_c}{dt} = \frac{dn_o}{dt} = -\frac{dn_{co}}{dt} \qquad (2.24)$$

Previously, Turkdogan and Vinters (1970) proposed that the rate for complete internal burning is given by Equation 2.25, as follows:

$$-\frac{dn_c}{dt} = n_c \frac{\Phi_1(p_{co_2} - p_{co_2}{}^c)}{1+\left(\frac{p_{co}}{\phi_{co}}\right)} \tag{2.25}$$

Integrating Equation 2.25 above for the boundary conditions, t=0, n=n0, when t=t, n=n_c yields

$$n_c = n^o \exp[\frac{\Phi_1(p^c{}_{co_2} - p_{co_2})}{1+\left(\frac{p_{co}}{\phi_{co}}\right)} t] \tag{2.26}$$

The rate of carbon consumption may be expressed by Equation 2.27

$$(\frac{dn_c}{dt})_{C-g} = n_C^o[\frac{\Phi_1(p_{co_2}{}^c - p_{co_2})}{1+\left(\frac{p_{co}}{\phi_{co}}\right)}]\exp[\frac{\Phi_1(p_{co_2}{}^c - p_{co_2})}{1+\left(\frac{p_{co}}{\phi_{co}}\right)} t] \tag{2.27}$$

Furthermore, King employed the model of Barati and Coley (2006) to calculate the oxygen supply rate at the slag-gas interface. The area of the slag-gas interface, $A_{sl,}$ can be calculated from the volume of gas generated inside the bubble resulting in equation 2.28

$$A_{sl} = (36\pi)^{1/3}(\frac{M_{CO}}{\rho_{CO}})^{2/3}(n_c^o - n_c)^{2/3} \tag{2.28}$$

This area can be combined with the rate equation of Barati and Coley to give:

$$-\frac{dn_O}{dt} = A_{sl}k_a(p_{CO}a_O - p_{CO_2}) = -\frac{dn_c}{dt} \tag{2.29}$$

$$p_{CO_2} + p_{CO} = 1 \tag{2.30}$$

where Φ_1 is the temperature-dependent carbon rate parameter [atm^{-1} min^{-1}], ϕ_{CO} is temperature-dependent carbon rate parameter related to carbon surface adsorption by CO [atm], p_{CO2} is the equilibrium pressure [atm] of CO_2 in bubble surrounding the carbon, p^c_{CO2} is the pressure of CO_2 at the carbon-gas interface [atm]. $n°_C$ is the initial number of moles of carbon in a particle, M_i and ρ_i are molar mass and density of CO and CO_2 respectively, a_O is equilibrium CO/CO_2 partial pressure in slag, Rp is the carbon particle injection rate [particles s^{-1}], k_a is the rate constant for reaction at the slag-gas interface [mol m^{-2} atm^{-1} s^{-1}], a_o is the oxygen activity of the slag, A_{sl} is the slag-gas interfacial area [m^2] and t is the carbon particle residence time in the slag[s].

Combining equations 2.27, 2.28, 2.29 and 2.30, King calculated the slag-gas-carbon reaction rate, and estimated CO_2 partial pressure inside the bubble.

King assumed bubbles are spherical and the instantaneous average diameter was calculated as shown in Equation 2.29

$$d_b = [\frac{(36\pi)^{1/3}}{\pi}(\frac{M_{CO}}{\rho_{CO}})^{2/3}(n_c^o - n_c)^{2/3}]^{1/2} \tag{2.31}$$

King (2009) was able to calculate the instantaneous rate for a single particle with a given residence time in the slag. He then calculated the overall rate of carbon gasification by multiplying the rate for each possible residence time by the number of particles at that residence time, and summed the over all possible residence time. R_p is the number of

carbon particles injected per time(s). The final multiple carbon particles injection model is given by:

$$(\frac{dn_c}{dt})_{C-g}^{tot} = R_p n_c^{\ o}\left(-1+\exp(\frac{\Phi_1\phi_{co}(p_{co_2}^{\ c} - p_{co_2})}{1+\phi_{co}+p_{co}}t)\right) \tag{2.32}$$

$$n_C^{tot} = R_p n_c^{\ o}(\frac{1+\phi_{co}+p_{co}}{\Phi_1\phi_{co}(p_{co_2}^{\ c} - p_{co_2})})\left(-1+\exp(\frac{\Phi_1\phi_{co}(p_{co_2}^{\ c} - p_{co_2})}{1+\phi_{co}+p_{co}}t)\right) \tag{2.33}$$

King then compared results from this model to his experimental data. The relationship is shown below for one of his experiments. The rate constant used for carbon gasification in King's model was that measured by Turkdogan and Vintners (1970) for metallurgical coke. This offered reasonable agreement with the gasification rates measured during injection but less after injection ceased (138s in Figure 2.6). King reasoned that this was because he had not used metallurgical coke in his experiments and that the carbon may well have been significantly more reactive. King adjusted the rate constant for carbon gasification, within the limits of values reported in the literature, until he obtained the best fit to his data. The result of the model using this "adjusted carbon reactivity" is also presented in Figure 2.6. As can be seen from the figure, this value is only important in predicting transient reaction rates and has no influence on the stead state gasification rate.

However, King found that the assumed reactivity of carbon had a major influence in the prediction of the steady state carbon content in the slag.

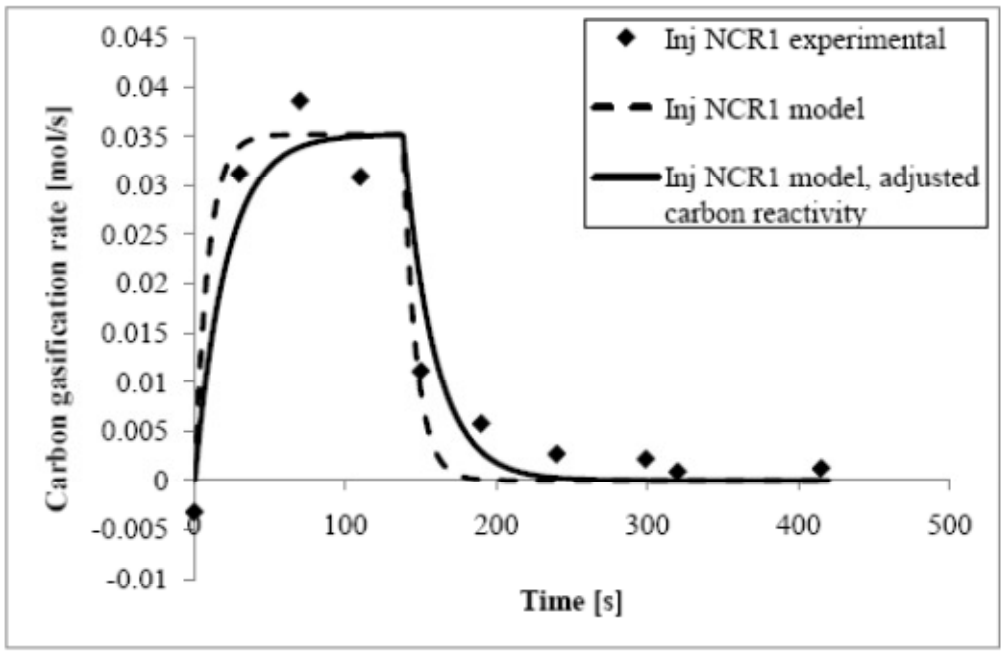

Figure 2. 6 Carbon gasification rates vs. time (King, 2009)

The prediction results of average bubble size shown in Figure 2.7 are inconsistent with most measurements and with other researchers; hence King's (2009) model may need further improvement in this regard. Since bubbles do not last infinitely, consideration of bubble rupture rate may play an important role in bubble size estimation.

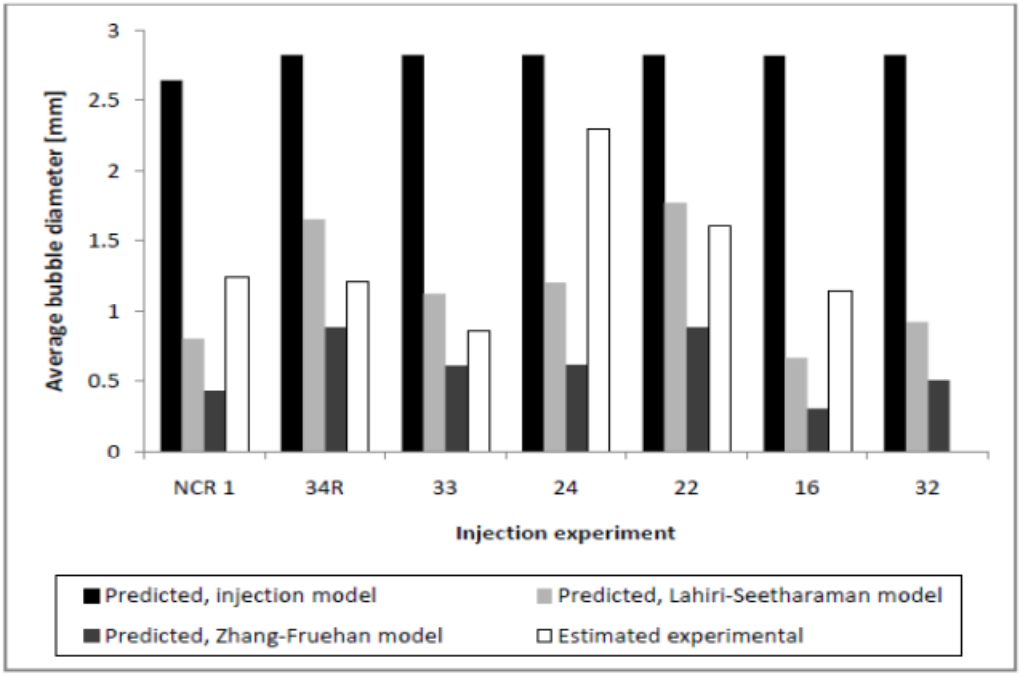

Figure 2. 7 Average bubble diameter prediction (King, 2009)

2.2.5 Bubble Wall Thickness

J. van der Schaaf and Ruud G. C. Beerkens (2006) discussed gas foaming in glass-melting processing. They outlined parameters that have an influence on bubble bursting rate such as bubble radius, physical properties of liquids, and interfacial mobility of foam. Their research also analyzed the relationship between mobility of foam and bubble life time or foam drainage rate. Moreover, a single critical bubble wall thickness (t_c) had been proposed, which originated from A. Vrij (1966). The original research suggests that bubble stability is dependent upon gravity and suction at the Plateau-borders when bubble wall thickness is high, and is dependent upon Van der Waals attraction (accelerates

bubble rupture rate) and double layer repulsion (reduces bubble rupture rate) when bubble wall thickness is low. An empirical relationship among the bubble wall thickness (t_c), the Hamaker Constant (A_H), the interfacial tension (σ), and an experimental value (Λ), was proposed as follows:

$$t_c = \left(\frac{A_H \Lambda^2}{128\pi\sigma}\right)^{0.25} \tag{2.34}$$

The value of Λ was then estimated as 0.21 r, where r is the bubble radius [m].

Furthermore, van der Schaaf and Beerkens (2006) concluded that the critical bubble wall thickness is given by:

$$t_c \approx 0.11\left(\frac{A_H d^2}{4\sigma}\right)^{0.25} \tag{2.35}$$

Where A_H is the Hamaker constant, d is the average bubble diameter, and σ is the surface tension of the liquid.

The Hamaker constant is used in calculating the dispersion force between two interacting materials. Gregory (1969) tried to estimate this constant for various materials by microscopic and macroscopic methods. The results obtained by these methods mostly differ by a factor of $3\pi/4$. Furthermore, Viseer (1972) and Gregory (1969) reported that most oxides have a Hamaker constant in the range 10^{-20} to 10^{-18} [J].

2.2.6 Bubble Structures

Bikerman (1972) conducted an extensive study of different types of foam, primarily spherical foam and polyhedral foam. The structure of these foams is shown schematically in Figure 2.8.

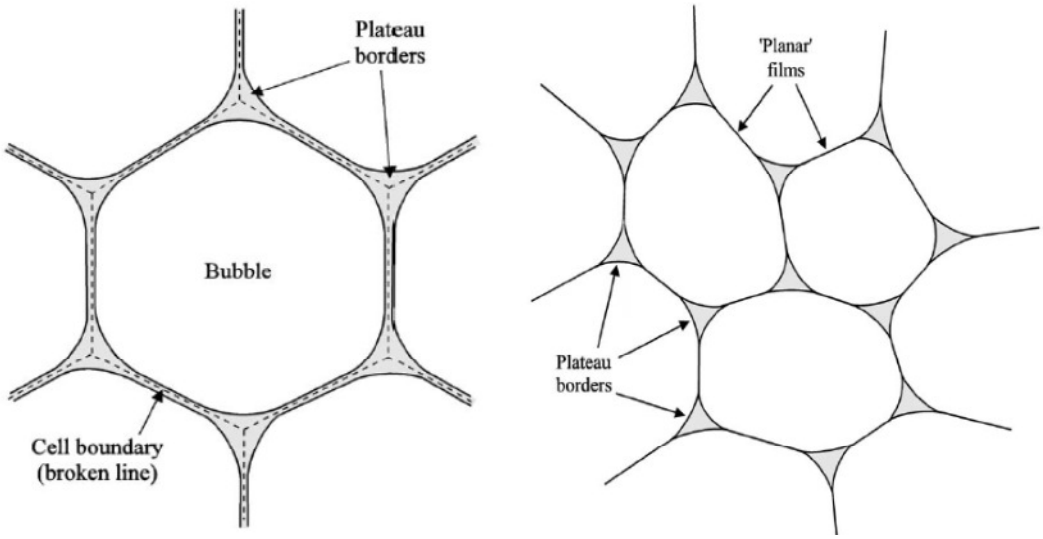

Figure 2. 8 Schematic of foam structure (P.M. Ireland, 2009)

In general, spherical foam consists of mostly spherical shape single bubbles and polyhedral foam is composed of random or planar shaped bubbles. The junction between three bubbles is called the Plateau border which interconnects the "cell boundaries" (or lamellae) in a triangular joint. According to the observations of Bikerman (1972), polyhedral foam has a higher rupture rate because the change of curvature in the lamellae is greater. They typically support less pressure than spherical shaped bubbles. Therefore, polyhedral foam is a metastable foam. It is very difficult to control and model this type of

foam. Moreover, gravity and capillary forces are significant factors in controlling single bubble drainage. These competing forces may lead to slower bubble rupture. On the other hand, thermal shock, chemical reaction, and turbulence can easily decrease foam stability.

2.2.7 Slag Viscosity

Slag viscosity is strongly dependent upon the slag structural unit (SU), temperature and composition. A model for the viscosity of Al_2O_3-CaO-"FeO"-SiO_2 slag was developed by Kondratiev and Jak (2001) and Iida et al. (2000). Most recently, Kondratiev and Jak (2005) found that applying a Quasi-Chemical thermodynamic model and using the Eyring equation offered excellent agreement with experimental results. This model was based on Frenkel's kinetic theory of liquids, which describes the liquid as showing a similar structure to a solid with molecules oscillating to close-by positions. The viscosity equation is:

$$\eta = \frac{2RT}{\Delta E_v} \frac{(2\pi m_{su} kT)^{0.5}}{v_{su}^{2/3}} \exp(\frac{E_a}{RT}) \qquad (2.36)$$

R- Gas constant (J/mol/K)

k- Boltzmann constant (J/K)

ΔE_v - Vaporization energy (J/mol)

E_a - Activation energy (J/mol)

m_{su} - Structure unit weight (kg)

v_{su} -Structure unit volume (m^3)

Kondratiev and Jak (2005) developed formulae to calculate the structural unit volume and the structural unit weight in binary metallic oxide- SiO_2 systems. These workers also summarized average SU weight and volume data for the slag system Al_2O_3-CaO-"FeO"-SiO_2 They also extrapolated vaporization energy and activation energy from their results.

In comparison to the Urbain model (2001), given in equation 2.37, the Quasi-chemical viscosity model yields better predictions of slag viscosity and can be broadly applied to a range of slag compositions.

$$\eta = AT\exp(\frac{1000B}{T}) \qquad (2.37)$$

The Urbain model has been presented in detail by King Thesis (2009).

2.2.8 Surface Tension

The surface tension of a liquid is the driving force to curtail its surface area and it plays an important role in slag foaming. Surface tension of slags and other oxide melts have been researched and discussed over the last several decades. The fundamental calculation

is mostly based on Butler's equation (1932). An evaluation of the surface tension of binary and ternary slag systems was conducted by Mills and Keene (1987). The surface tension of a mixed oxide melt can be computed as the sum of each partial surface tension and can be formulized as follows:

$$\sigma = \sum_{i=1}^{n} X_i \sigma_i \qquad (2.38)$$

X_i - molar fraction of component i

σ_i - partial molar surface tension of component i

The partial surface tension values obtained by Mills and Kneene (1987) are presented in Table 2.2.

Table 2. 2 Partial molar surface tension of slag composition at 1773 K (Mills and Keene, 1987)

Component	**Al_2O_3**	**CaO**	**FeO**	**MgO**	**MnO**	**SiO_2**	**TiO_2**
σ_i (mN/m)	655	625	645	635	645	260	360

The calculation of surface tension at temperatures other than 1773K was given as follows:

$$\sigma = \sigma_{1773} + [\frac{0.15}{1000}(T - 1773)] \qquad (2.39)$$

Nakamoto (2007) reported surface tension for Al_2O_3, CaO, FeO, MgO and MnO as a function of temperature T (K) in the range from 1473 K to 1873 K. These data are presented in Table 2.3.

Table 2. 3 Slag surface tension prediction (Nakamoto, 2007)

Composition	σ_i **(mN/m)**	**Temperature range**
Al_2O_3	1024 - 0.177T	1473-1873**K**
CaO	791 - 0.0935T	1573-1873**K**
FeO	504 + 0.0984T	1473-1873**K**
MgO	1770 - 0.636T	1623-1873**K**
MnO	988 - 0.179T	1673-1873**K**

In comparison to the data of Mills and Keene, that of Nakamoto has mostly higher values except for CaO, which is exactly same at 1773K. Nakamoto is applicable over a limited temperature range; therefore, whilst it may be more accurate, it can be less broadly used.

2.2.9 Density

Density of slag has been studied by Mills and Keene (1987) who proposed models to estimate density using molar volume, calculated from partial molar volumes, and molar mass. The basis of this calculation is given in Equation 2.40.

$$V = \sum_{i=1}^{n} X_i V_i = \frac{\sum_{i=1}^{n} M_i X_i}{\rho} \qquad (2.40)$$

X_i - molar fraction of component i

V_i - partial molar volume of component i

M_i - molar mass of component i

Values of partial molar volume recommended by Mills and Keene for use in calculating slag density are presented in Table 2.4.

Table 2. 4 Partial molar volumes of slag components at 1773 K (Mills and Keene, 1987)

Components	V_i ($cm^3 mol^{-1}$)
Al_2O_3	28.31+32 $X_{Al_2O_3}$ - 31.45 $X^2_{Al_2O_3}$
CaO	20.7
FeO	15.8
MgO	16.1
MnO	15.6
SiO_2	19.55 + 7.966 X_{SiO_2}

$$V = V_{1773} + [\frac{V_{1773}}{0.0001}(T - 1773)] \quad (2.41)$$

Olivares et al. (1991) compared slag density before and after annealing processing at 1573K. They proposed Equation 2.42 for the density of unannealed slag:

$$\begin{aligned}\rho = 2.93 + 0.0041(wt\%CaO) - 0.00437(wt\%SiO_2) - 0.00299(wt\%Al_2O_3) \\ -0.00475(wt\%Na_2O) + 0.00299(wt\%CaF_2)\end{aligned} \quad (2.42)$$

Each of these models applies within a defined composition and temperature range. In the present work, the model of Mills and Keene (1987) has been chosen because it is appropriate for the slag compositions employed in this work.

2.2.10 Effects of Slag Properties on Foaming

Ogawa et al. (1993) researched slag properties on foaming and developed a physical model to describe foaming. The main concept is shown in Figure 2.9, they calculated gas generation rate, foam rupture rate and bubble distribution (void fraction) which in combination can be used to evaluate foam height.

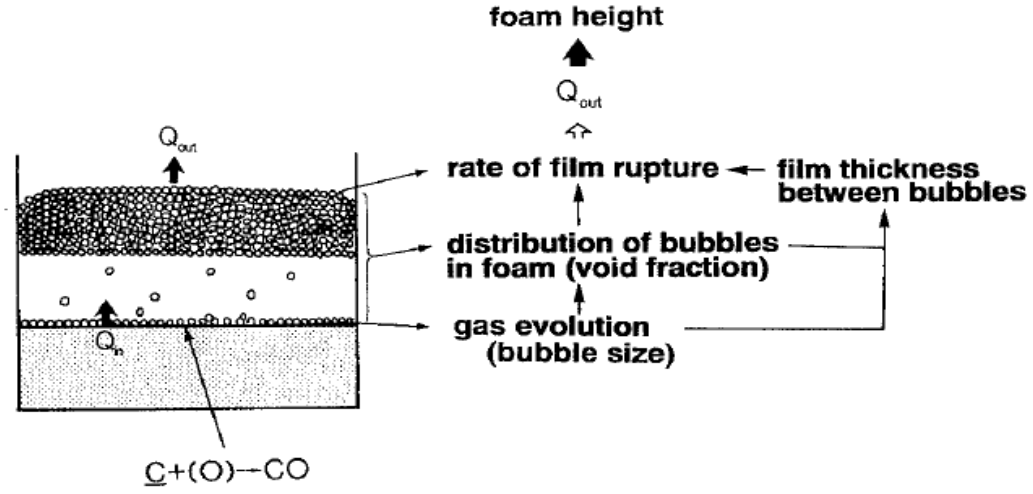

Figure 2. 9 Slag foaming model (Ogawa et al. 1993)

Ogawa et al. (1993) conducted experiments to estimate the relationship between foam void fraction and superficial gas velocity, bubble size and surface tension, bubble size and gas escape rate, and the change rate of foam height and bubble size. The findings of their experiments are summarized in the following table.

Table 2. 5 Effects of slag properties in foaming model (Ogawa et al. 1993)

	Foam height	**Bubble rupture rate**	**Bubble size**	**Void fraction**
Slag Viscosity (μ) **increase**	**increase**	**decrease**	**N/A**	**decrease**
Surface tension (σ) **increase**	**decrease**	**increase**	**increase**	**increase**
Slag-metal interfacial tension- **increase**	**decrease**	**increase**	**increase**	**increase**
Surface tension of metal-**increase**	**increase**	**decrease**	**increase**	**decrease**

Most recently, Wu et al. (2010) extensively studied the effect of viscosity in slag foaming. Their physical modeling work, using silicone oils, shows that foam height only increases with viscosity in a certain range. After some critical value of viscosity, further increases result in a decay of foam height. Meanwhile, small solid particles, for instance carbon or coal, only benefit slag foaming at relatively low concentrations where they increase effective viscosity. Excessive numbers of small particles possibly decrease the tendency for slag foaming.

2.3. Coal Oxidization

Story and Fruehan (2000) suggested that in oxidation of carbon mass transport and chemical reaction will affect the reaction rate, activation energy and reaction order. They summarized three possible rate determining regimes:

1) **Chemical kinetic control;** when reaction take places at low temperatures, diffusion in the pores has a higher rate than chemical reaction at the surface, hence activation energy and reaction order are determined by chemical kinetics.
2) **Limited mixed control regime**; when the reaction occurs at higher temperatures, the rate is most likely controlled by a combination of diffusion within the pores and chemical reaction at the pore surface. The transition between regimes 1 and 2 is also dependent upon coal particle size and gas concentration gradient. According to the model proposed by Zeldowitsch and Frank-Kamenetskii (1969), based on Thiele's theory (1939), the rate can be formulated as:

$$J_i^{pore} = \sqrt{D_e \rho S k_i C_s} \qquad (2.43)$$

where D_e is effective diffusivity, ρ is the density of the reaction layer, S is surface area of pore per unit mass, k_i is the intrinsic rate constant, C_s is gas concentration at the coal surface.

3) **External diffusion control** occurs at even higher temperatures, where diffusion of gas to the coal particle surface controls the rate, and the activation energy here is very

low in keeping with gas phase diffusion.

Story and Fruehan (2000) suggested that external diffusion control and limited mixed control are the most likely mechanisms at relatively high temperatures (1300° C -1500° C), assuming coal particle size is sufficiently large. Turkdogan (1968, 1969 and 1970) proposed that the size threshold of graphite particles for complete internal burning is up to 2.0 mm, and for partial internal burning is at least 7.0 mm. These estimates were for 1100° C. Coke and coal are more porous than graphite; therefore, one would expect the transition from complete internal burning to occur at higher temperatures and larger particle sizes. Furthermore, Turkdogan (1968) investigated complete internal burning, carbon oxidation, and emphasized that rate of oxidization is strongly dependent on the size of carbon particle, the pressure of carbon dioxide and temperature. Turkdogan conducted experiments to evaluate the size effect for pore diffusion and chemical reaction kinetics by using particulate electrode graphite. By examining the effect of average graphite particle diameter versus reaction rate per particle (gC/min) at 900° C, 1000° C, 1100° C, and comparing the results in a diagram of the logarithm of oxidation rate per particle versus the logarithm of particle diameter, they proposed relationships for pore diffusion control where the slope is 2:1 and chemical reaction control where the slope is 3:1. When the rate is controlled by pore diffusion, decreasing carbon particle size leads to increased rates whereas, the rate is independent of particle size below some critical dimension, where internal burning dominates.

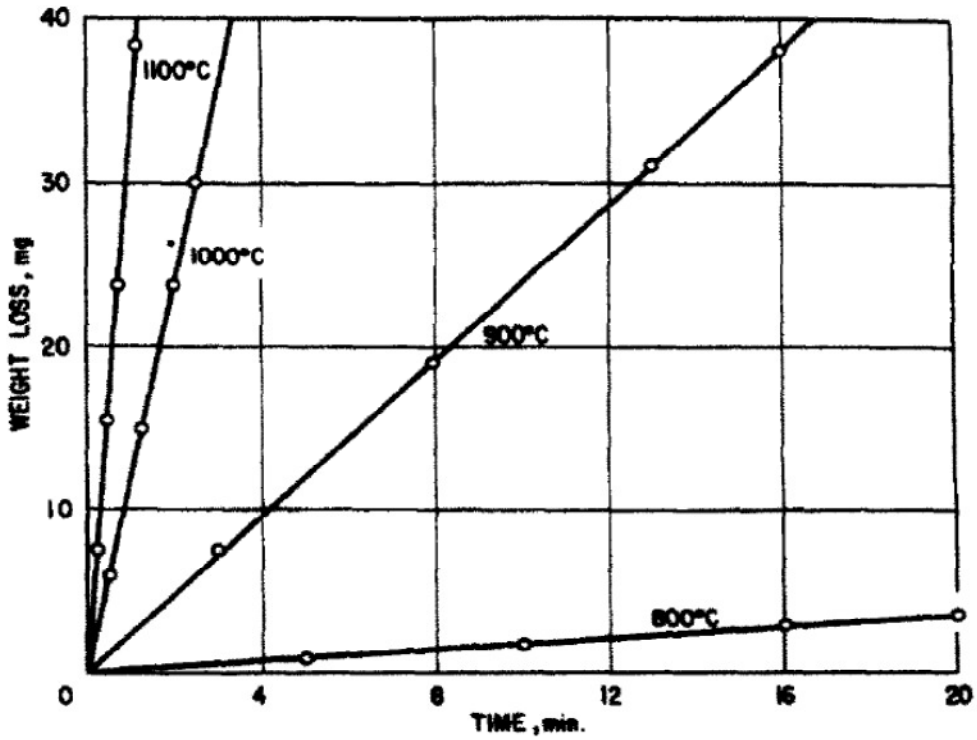

Figure 2. 10 Temperature effect on oxidation of coconut charcoal particle at 0.96 atm CO_2 (Turkdogan, 1969)

This research concluded that complete internal burning is favored by small particle size, low carbon dioxide pressure and low temperature, and CO has a strong poisoning effect for oxidization.

Turkdogan and Tien determined a reaction rate parameter Φ from experimental results and concluded that Φ is proportional to the specific surface area of the carbon and $\log\frac{\Phi}{T}$ is inversely proportional to temperature.

Coconut charcoal: $$\log\frac{\Phi}{T} = -\frac{14800}{T} + 7.80 \qquad (2.44)$$

Electrode graphite $\log\frac{\Phi}{T} = -\frac{14800}{T} + 5.50$ (2.45)

A mathematical model was developed by Turkdogan and Vinters (1970),

$$R = \frac{\Phi_1[(p_{CO_2}) - (p_{CO_2})_e]}{1 + (\frac{p_{CO}}{\phi_{CO}})} \quad (2.46)$$

$$p_{CO} = \phi_{CO}\frac{\theta_{CO}}{1-\theta_{CO}} \quad (2.47)$$

θ_{CO} - Fraction of sites occupied by CO
$(p_{CO_2})_e$ -Equilibrium pressure
Φ_1 - Reaction rate parameter
ϕ_{CO} - Activity coefficient for adsorbed CO

For metallurgical coke, Turkdogan evaluated the temperature dependence of Φ.

$$\log\Phi_1 = -\frac{13200}{T} + 8.60 \quad (2.48)$$

$$\log\Phi_2 = -\frac{15000}{T} + 9.98 \quad (2.49)$$

$$\log\phi_{CO} = -\frac{5940}{T} + 3.46 \quad (2.50)$$

2.4 Summary of the Literature

Slag foaming studies have focused on two major aspects: kinetics of reaction of carbonaceous materials, and the effects of slag properties on foam. Many researchers simulated slag foaming over a wide range of slag composition, gas generation rates and temperature. Some, limited data have been obtained from industrial EAFs, then analyzed and compared with work accomplished in laboratories.

King, 2009, developed a kinetic model which successfully predicted instantaneous slag foaming and kinetic parameters in laboratory scale. This model supplies a preliminary blueprint to simulate carbon injection into EAF slags. By combining this with the work of Fruehan and co-workers and Lahiri it is possible to predict foaming. However, King's work does not provide a good estimate of bubble size in the foam and shows a change in the relationship between superficial gas velocity and foam height which is not predicted by the foaming index concept. The current work is focused on explaining this change which occurs at high foam heights. The mechanism by which this occurs will be discussed and explained by considering slag volume and changes in bubble size, and bubble wall thickness.

Chapter 3: Experimental

3.1 Coal Injection Experiments

The experimental methods employed in the current work were designed and employed in previous work (King, 2009, Ji and et al. 2005) to simulate carbon injection into EAF slags and observe slag foaming phenomena. A schematic of the experimental apparatus is shown in Figure 3.1. Experimental procedures are described as follows:

Metal and slag were heated using a 75 kW induction furnace, with an MgO crucible, interior diameter 191 mm and height 295 mm. Slags were prepared from oxide powder and added gradually to the surface of preheated steel. The weight of steel was approximately 15.9 kg and the experimental temperature was around 1900 K. The height of liquid steel and slag were separately measured by inserting a steel rod into the completely melted liquid. When the slag was melted thoroughly, a stainless steel lid and ceramic fiberboard were set up over the crucible as shown in Figure 3.1. An injection lance was inserted through the center of the lid and immersed in the slag to an approximate depth of 31.8 mm(1-1/4 inches) under the slag surface. 1NL•min^{-1} nitrogen was used to purge air from the furnace before injecting coal. The flow rate was increased to 7.7±0.3 NL•min^{-1} during coal injection. Using gas-tight syringes, gas samples were collected from the exhaust pipe throughout the injection process.

The slag was prepared by mixing powders in the following weight proportions: 42.0 pct CaO, 23.4 pct FeO, 5.7 pct Al_2O_3, 21.6 pct SiO_2 and 6.4 pct MgO. The instantaneous composition was obtained from ICP measurements of multiple time sampling. Slag and steel samples were obtained by multi-depth silica suction-pipes before, during and after coal injection. A Perkin Elmer AutoSystem XL Gas Chromatograph was used to analyze all gas samples for CO, N_2, CO_2, H_2 and O_2. A computer system collects signals of major off-gas components (CO, CO_2 and O_2), weight of coal, carrier gas flow rate, real sampling time, carbon injection start and end time at 0.5 second intervals.

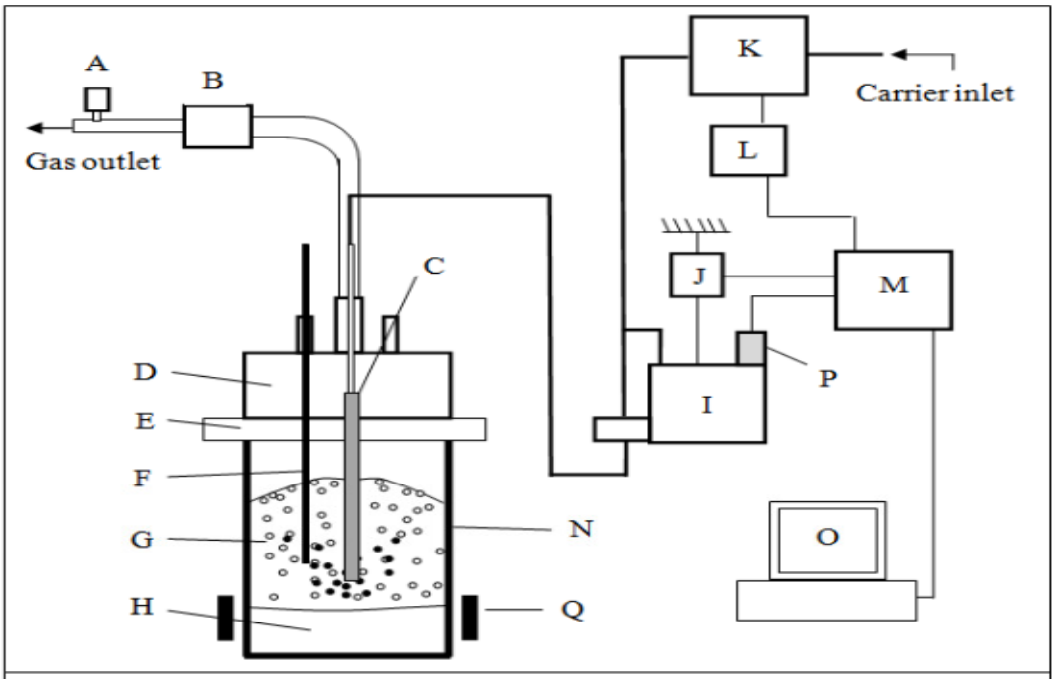

A – Gas sample port; B – Filter; C – Lance; D – Lid; E – Ceramic fibreboard; F – Steel rod; G – Slag; H – Steel; I – Feeder; J – Load cell; K – Flow rate transducer; L – Flow meter; M – A/D card terminal; N – High-MgO Crucible; O – Computer; P – Pressure transducer; Q – Graphite ring

Figure 3. 1 Coal Injection experimental set up (King, 2009)

3.2 Experimental Materials

Metal (low carbon steel 0.003 wt% C supplied by Dofasco) and pre-mixed oxide powders (Calcium oxide, Mill Scale, Calcined Alumina, Magnesite, Silica Quartz Sand) are used in all experiments. The composition of these materials is listed in Table 3.1

Table 3. 1 Oxide powder detailed composition

Wt%	**Calcium Oxide**	**Mill scale**	**Calcined Alumina**	**Magnesite**	**Silica quartz sand**
CaO	>98.24	-	-	1.68	-
Al_2O_3	-	-	99.5	0.99	-
MgO	-	-	-	93.66	-
SiO_2	-	-	0.05	2.38	99
Iron(Fe)	<0.1	-	-	-	-
FeO	-	51.8	-	-	-
Fe_3O_4 **Fe_2O_3**	- -	45.9 -	- 0.05	- 1.29	- -
Chloride(Cl)	<0.005	-	-	-	-
Nitrate(NO_3)	<0.005	-	-	-	-
Sulphate (SO_4)	<0.1	-	-	-	-
Heavy metals (as Pb)	<0.004	-	-	-	-
Na_2O	-	-	0.35	-	-

The slag was weighed to a 0.5 g error for each oxide and mixed thoroughly before adding it to the furnace. Hence accumulated error for mixed slag is 2.5 g. The designed composition of slag is shown in table 3.2:

Table 3. 2 Components of slag

Oxides Powder	**Magnesite**	**Mill Scale**	**Silica Quartz Sand**	**Calcined Alumina**	**Calcium Oxide(Lime)**	**Total**
Designed Weight(g)	232.5	770.5	778.0	205.0	1594.5	3580.5

Meanwhile we assume that 75 g extra FeO is obtained from the oxidation of steel during heating and Calcium Oxide contains approximately 3% moisture. All slag compositions are measured after melting and it is these real compositions that are used in any calculation of slag properties.

The average diameter of coal particles used in injection experiments is 0.216 mm. Coal was supplied by ArcelorMittal Dofasco. The details of the coal composition, coal size distribution and volatile content are given in tables 3.3, 3.4, 3.5.

Table 3. 3 Analyzed Dofasco coal composition (King, 2009)

	Fixed Carbon	**Volatile**	**Ash**	**Sulphur**	**Moisture**
wt %	90.52	3.88	3.96	0.49	1.15

Table 3. 4 Dofasco coal composition (King, 2009)

	Carbon	H_2	N_2	CO	CO_2	Ash	Sulphur	Moisture
wt %	91.72	0.75	0.93	0.56	0.44	3.96	0.49	1.15

Table 3. 5 Dofasco coal diameter distribution (King, 2009)

Mesh	SI, mm	Mass % (screening time 5 min.)	Mass % (screening time 20 min.)	Mean Mass %	Cumulative Mean Mass %
<200	<0.074	4.36	4.54	4.45	4.45
200-140	0.074-0.104	6.03	6.30	6.17	10.62
140-80	0.104-0.177	24.01	24.14	24.08	34.69
80-50	0.177-0.297	49.08	47.58	48.33	83.02
50-30	**0.297-0.595**	**9.95**	**10.79**	**10.37**	**93.39**
30-16	0.595-1.190	1.97	2.04	2.01	95.40
16-8	1.190-2.360	4.60	3.08	3.84	99.24
>8	>2.360	0	1.53	0.77	100.00

The carrier gas, 99.998% N_2, was used for all coal injection experiments.

3.3 Gas and Slag Analysis

Perkin Elmer Autosystem XL Gas Chromatograph was calibrated by blank gas, air, and two standard gases (3.78 % N_2 and 96.22% H_2 mixed gas, and 5% O_2, 7% He, 6.25% CO, 25% CO_2 and 56.75% N_2 mixed gas) before analyzing gas samples.

All slag samples were quenched immediately in water and then an ICP-OES system was used to analyze detailed compositions. Samples of frozen slag were photographed and image analysis software was used to determine average bubble size.

3.4 Temperature Control

The temperature of slag was measured before carbon injection after slag melting was completed, and also 8 to 9 minutes after carbon injection stopped. The furnace was adjusted to a target temperature of 1900 K if the first measurement was too high, and vice versa. Precise temperature control during carbon injection was not possible. And average temperature was used in analyzing the results. In most experiments temperature was maintained within +/- 20 K of the average for that experiment.

3.5 Experimental Errors

The source of errors in coal injection rate and measured gasification rate were discussed extensively in King's work (2009), such as blockage of lance resulting in an abrupt

change of gasification rate, coal particles floating on the slag surface reacting at a much slower rate than fully immersed coal inside the slag.

Furthermore, it is expected that injection depth and carrier gas flow rate have important influences on initial coal injection position relative to the slag-metal interface. It is difficult to control injection depth precisely in each experiment because of errors in measuring lance position, approximately 0.16 cm, and the position of the slag/metal interface is not identical in each experiment. When coal was injected closer to the slag/metal interface, more CO/CO_2 was produced in the reaction since coal particles have a longer time to react. Similarly, a higher carrier gas flow rate leads to deeper penetration also resulting in longer reaction times.

Analysis of gas and slag samples has various sources of error. The details of the uncertainty calculation were given by King (2009) as shown below:

$$\delta(Q_c) = \left|\frac{\partial(Q_c)}{\partial(C_{Inj})}\right|\delta(C_{Inj}) + \left|\frac{\partial(Q_c)}{\partial(Q_{N_2})}\right|\delta(Q_{N_2}) + \left|\frac{\partial(Q_c)}{\partial(\%CO_2)}\right|\delta(\%CO_2) + \left|\frac{\partial(Q_c)}{\partial(\%CO\ )}\right|\delta(\%CO\ )$$

$$+\left|\frac{\partial(Q_c)}{\partial(\%O_2)}\right|\delta(\%O_2) + \left|\frac{\partial(Q_c)}{\partial(\%N_2)}\right|\delta(\%N_2) + \left|\frac{\partial(Q_c)}{\partial(\%H_2)}\right|\delta(\%H_2)$$

The slag samples are analyzed by ICP-OES are usually calibrated to 10% uncertainty each element, but typical error range after removing high error data (greater than 10%) is from about 1% to 7%, hence we may conclude that uncertainty in slag composition is

within the range of 5%. The slag may not be homogeneous, particularly when foamed. Therefore there could be an error introduced based on the point at which a sample was taken.

The measurement of foam height has 0.64 cm error.

Error of time recording, furnace temperature controlling, leakage of syringe and melting of slag are other minor factors compared with those discussed above.

Chapter 4: Experimental Analysis and Results

4.1 Calculation of Foam Index and Average Bubble Size

The slag foam index is the ratio of foam height to superficial gas velocity, in units of [s]. The foam height in the present work is measured, experimentally, superficial gas velocity is calculated from the maximum gasification rate.

Experimental average bubble size was measured by scanning frozen slag samples and then using volume-average calculation from results of measured bubble sizes. King (2009) discussed the accuracy of this method to determine average bubble size and further improvement may be needed to obtain more precise results.

Similarly, in the present work multiple angle imagines are taken of experimental slag samples, which are directly analyzed using image analysis software. Although this method is easier and can test a much larger number of bubbles, the 3-dimensional sample is difficult to observe properly in a 2-dimensional imagine because of the non-uniform surface. The difference between high temperature liquid bubbles and frozen slag samples is another uncertainty in our approach to the measurement of bubble size. The phenomenon of slag falling after cooling slag was mentioned in King's thesis also occurred frequently in the present work; therefore, measuring bubble size is not possible for every experiment.

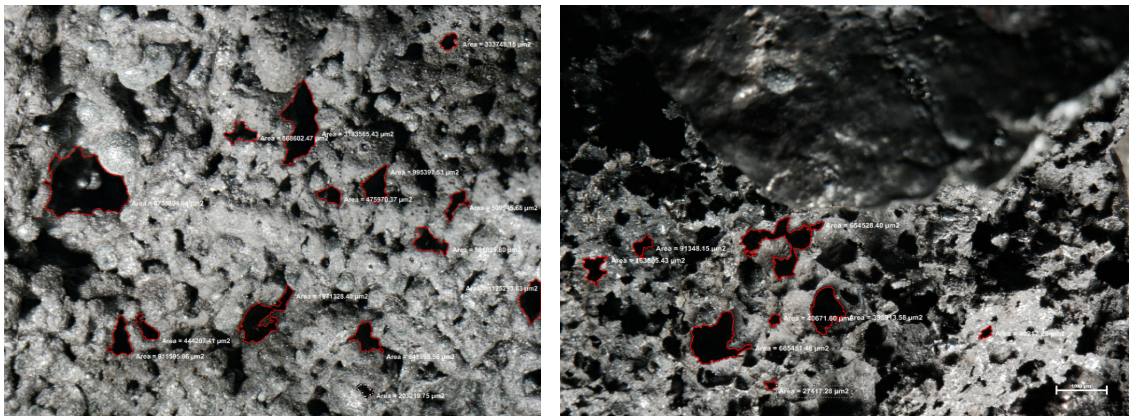

Figure 4. 1 Imagines of frozen slag samples analyzed by imagine software

4.2 Experimental Results

The relationship between superficial gas velocity and slag foam height is plotted in Figure 4.2 which includes data from King (re-analyzed to correct errors in calculation of superficial gas velocity, experiments 16, 22, 24, 33, 34, 35) as well as data from the present work (experiments 36, 37, 38, 39).

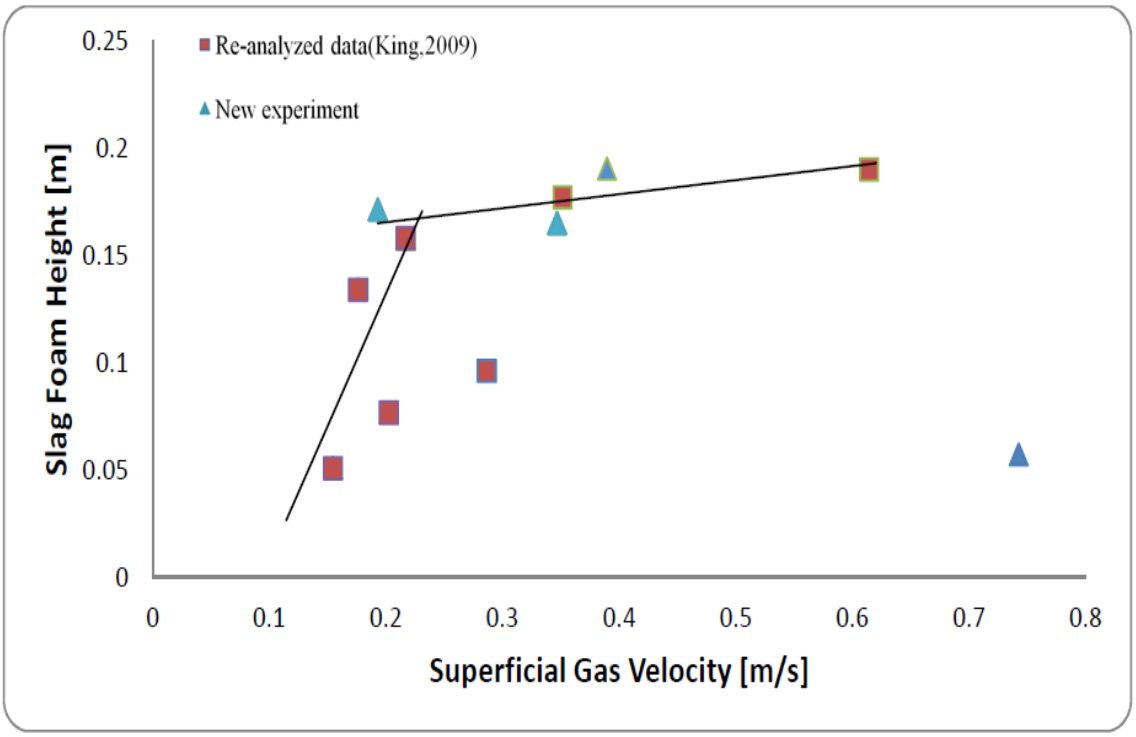

Figure 4. 2 Slag foam height vs. superficial gas velocity

Table 4.1 provides carbon injection rate, maximum carbon gasification rate, slag foam height and foam index for injection experiments 16, 22, 24, 33, 34, 35, 36, 37, 38, 39. The detailed calculation of off gas composition from gas chromatography data and maximum gasification rate are given in Appendix A.1.

Table 4. 1 Experimental Results

	Exp. 16	**Exp. 22**	**Exp. 24**	**Exp. 32**	**Exp. 33**	**Exp. 34**
Carbon injection rate [mol s^{-1}]	0.0338	0.0359	0.0338	0.0391	0.0566	0.0749
Maximum carbon gasification rate [mol s^{-1}]	0.0270	0.0512	0.0360	0.0325	0.0646	0.1127
Slag foam height [m]	0.0508	0.0962	0.0767	0.134	0.177	0.190
Foam index [s]	0.329	0.335	0.379	0.762	0.504	0.309
Temp. [K]	1991	1941	1959	1888	1895	1900

Table 4. 2- Experimental Results

	Exp. 35	**Exp. 36**	**Exp.37**	**Exp. 38**	**Exp.39**
Carbon injection rate [mol s^{-1}]	0.0352	0.0484	0.0675	0.0576	0.0561
Maximum carbon gasification rate [mol s^{-1}]	0.0398	0.0357	0.1421	0.0635	0.0701
Slag foam height [m]	0.158	0.171	0.0572	0.165	0.191
Foam index [s]	0.729	0.889	0.077	0.476	0.329
Temp. [K]	1900	1903	1822	1886	1938

It is clear from Figure 4.2 that increasing carbon injection rate does not maintain a constant incremental increase in slag foam height. The critical height was found to be approximately 0.168 m for the slag volume employed in this work. This result is contradictory to previous publications from Fruehan et al. (1991, 1995), Lahiri and Seetharaman (2002), which mostly concluded that superficial gas velocity vs. foam height maintained one linear relationship throughout the slag foaming process if slag composition and volume were fixed. According to Fig. 4.2 there were two outstanding results; Exp. 22 and Exp. 37, show significant departure from the main tendency line. In the case of Exp. 37, it appears that an extremely high carbon injection rate led to low foam height. In the case of Exp. 22, there was poor control of temperature and slag volume which would explain the anomalous result. The phenomenon behind the behavior in Exp. 37 is probably related to an excess of carbon particles in the foam.

Carbon injection rate and the resulting maximum gasification rate were likely in linear relationship as suggested in King's work (2009). The foam indices in the current work are 0.309 s to 0.889 s. They are relatively similar to those considered in Jiang and Fruehan's research (1991), which were 1.3 s and 0.6 s in laboratory work, and 0.61 s to 0.81 s in industrial scale bath smelting experiments. However, the current foaming indices are smaller than those of Lahiri and Seetharaman (2002), which were in the range of 1-2 s in laboratory work, and Matsuura and Fruehan (2009) who studied slags with foam indices of 2-4 s and 6-8 s in an industrial EAF furnace. Therefore, experimental conditions in the current work are comparable to previous work by other researchers, and bubble size, slag composition and gas generation rate would be expected to follow similar trends.

Chapter 5: Discussion

5.1 Optimum Carbon Injection Rate

In previous work (King, 2009), the carbon gasification rate was found to be strongly dependent on the carbon injection rate in the range of temperature (1821K<T <1991K). The height of foaming slag was dependent upon superficial gas velocity, which was dependent on experimental carbon gasification rate and hence controlled by carbon injection rate. Figure 4.2 demonstrates that at some critical height, there is a dramatic departure from the initial linear relationship between foam height and superficial gas velocity. Above this critical point, foam height continued to increase as a function of superficial gas velocity but at a greatly diminished rate.

The molten slag used for slag foaming is observed to be a strongly foamy solution, and its foam is beer-like and polyhedral or spherical structure. The foam is assumed to have an approximately constant void fraction and it grows by adding more liquid. At some point, all the liquid will be consumed and the foam can only grow by increasing the void fraction. The apparent discrepancy in superficial gas velocity vs. foam height may be explained if the amount of slag available for foaming is limited, and the gas velocity is sufficient to consume all or most of the liquid slag. In order to generate additional foam, the diameter of existing bubbles must be increased or new bubbles must nucleate from the liquid film between bubbles. Thinner walled bubbles will have a greater tendency to burst or coalesce. In either case, it is expected that the formation of new foam will become

more difficult due to less available liquid slag and there will be a higher risk of bubble rupture. Both of these effects will result in a smaller increase in foam height for a given incremental increase in superficial gas velocity.

The optimum carbon injection rate is the point at which superficial gas velocity reaches the critical point for a given slag volume. At this point, it is assumed that all molten slag has been consumed to generate foam. This critical point has rarely been observed because previous studies have used a much smaller superficial gas velocity relative to the amount of slag. However, recent work by the author Zhu, Coley, Irons and Ray (2011) has shown that in industrial furnaces, conditions may exceed the critical foam height.

In order to understand the mechanism of slag foaming beyond the critical point, the average bubble wall thickness is an important parameter. The bubble wall thickness prediction based on the work of J. Van der Schaaf and Beerkens (2006) was calculated by assuming the critical point observed in experiments 35 and 36, occurs when the slag is completely consumed to generate foam. This average critical wall thickness is expressed in equation 5.1:

$$t_{cri} = 0.11\left(\frac{A_H\left(\frac{d_{avg}}{2}\right)^2}{\sigma}\right)^{0.25} \qquad (5.1)$$

The assumptions adopted in the calculation of average bubble wall thickness are:

1. Each gas bubble is spherical in molten slag
2. All molten slag is consumed to construct foam when the carbon injection rate is greater than critical rate
3. The bubble wall is shared with an adjacent bubble
4. Volume of liquid surrounding bubbles is negligible because of $t_{cri} << d_{avg}$
5. Critical bubble wall thickness represents average bubble wall thickness after the critical point in Fig. 4.2 which means that all bubbles are either in steady-state or at the thickness immediately before bubble bursting.

Figure 4.1 shows that assumptions 1 and 4 are not true when frozen slag samples are observed in the room temperature. It is likely that the former still offers a reasonable approximation, however the latter assumption is likely to introduce significant error. This will be addressed later in this chapter.

Then the summation of liquid volume in each bubble is equal to the overall volume of liquid slag.

From $V_{slag}=V_{slag\_in\_foam}$

$$h_{slag}\pi(\frac{d_{cru}}{2})^2 = \frac{1}{2}N_b(\pi d_{avg}^2 t_{cri}) \qquad (5.2)$$

And the total number of bubbles entrained in the foam can be calculated as follows:

$$N_b = \frac{V_{foam}}{V_{avg\_bubble}} = \frac{(h_{slag} + h_{foam})\pi(\frac{d_{cru}}{2})^2}{\frac{4}{3}\pi(\frac{d_{avg}}{2})^3} \quad (5.3)$$

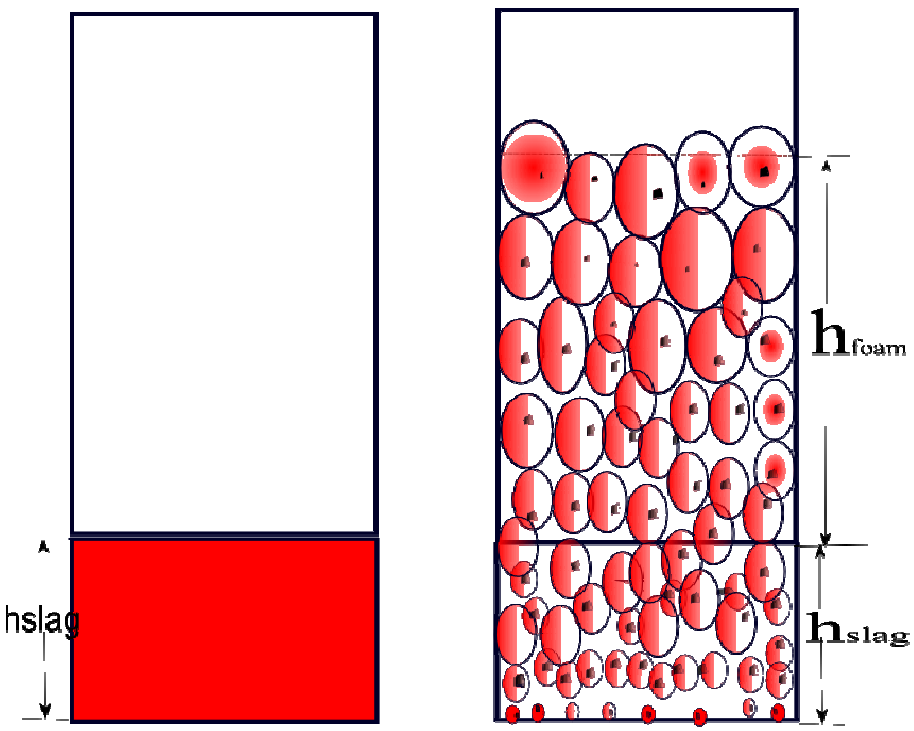

Figure 5. 1 Schematic of slag foaming before and after carbon injection in critical injection rate.

Where t_{cri} is equilibrium bubble wall thickness[m], A_H is the Hamaker constant in [J]., d_{cru} is the furnace crucible inner diameter, d_{avg} is the average bubble diameter[m], h_{slag} is the

molten slag height [m] before carbon injection, N_b is the total number of spherical bubbles in the slag at the critical point, h_{foam} is the foam height from measurement defined as the change of liquid slag level, and σ is the slag surface tension.

Consequently, the Hamaker constant is estimated by combining equations 5.1, 5.2 and 5.3 and is shown in equation 5.4

$$A_H \approx 337.3\left(\frac{h_{slag}}{h_{foam} + h_{slag}}\right)^4 d_{avg}^2 \sigma \qquad (5.4)$$

From the results of these experiments we conclude that the Hamaker constant is equal to 2.80×10^{-6}[J] if the method of Lahiri and Seetharaman (2002) is used to calculate the bubble size and 9.30×10^{-6} [J] if the method of Zhang and Fruehan (1995) is used. However this calculation disagrees with Viseer (1972) who estimated that most homogenous oxides have a Hamaker constant in the range 10^{-20} to 10^{-18} [J]. It should be noted that Viseer's estimates were for room temperature and that the higher temperatures employed in the current work and the mixture of different of materials may cause this to vary significantly. If we apply the foregoing method to estimate Hamaker constants from the data of Wu (2000), which was used in Lahiri-Seetharaman (2002) , and experimental results from Zhang and Fruehan (1995), we see reasonable agreement with the current work as shown in Table 5.1. It is may be well be reasonable to expect very different values for the Hamaker constant at high temperature compared to those

found at room temperature. However, care should be taken in reading too much into the data presented in Table 5.1. The Hamaker constant is used in describing the behavior of thin films, whereas the current work is based on foams with gas fractions less than 0.9 which would typically have fairly thick bubble walls.

Table 5. 1 Hamaker constant(A_H) approximations

Experiment	**Foam Height [m]**	**A_H (Lahiri-Seetharaman's model) [J]**	**A_H (Zhang-Fruehan's model) [J]**
Exp. 35	0.158	1.19×10^{-5}	3.45×10^{-6}
Exp. 36	0.171	7.94×10^{-6}	2.46×10^{-6}
Wu's[19] Research	0.080	1.92×10^{-5}	9.41×10^{-6}
Zhang's[7] Research	0.160	1.97×10^{-7}	8.02×10^{-8}
Zhang's[7] Research	0.088	6.22×10^{-6}	2.99×10^{-6}
Critical Point In Fig 4.	0.167	9.30×10^{-6}	2.80×10^{-6}

Furthermore, the expression of bubble wall thickness can be simplified as in equation 5.5 by combining equations 5.1 and 5.4.

$$t_{cri} \approx 0.33\left(\frac{h_{slag}}{h_{slag} + h_{foam}}\right) d_{avg} \qquad (5.5)$$

The molten slag height and foam height were measured in these experiments. Because bubble size could only be measured in a limited number of experiments, the average bubble size used to calculate wall thickness was estimated using the models of Lahiri and Seetharaman (2002) and Zhang and Fruehan (1995). Slag viscosity was calculated by using Urbain's model (2001), and slag density and surface tension were calculated by using Mills and Keene's models (1987). The average bubble wall thickness in all experiments except for Exp. 22 and 37 was estimated using equation 5.5. These results are plotted vs. foam height and are shown in Figure 5.2, although it is recognized that this method for predicting bubble thickness is not be valid below the critical foam height.

It is worth commenting on the experiments excluded from this analysis. Exp 22 showed very poor control of temperature and provides little useful insight. However, consideration of Exp 37 may offer some important insight. In the case of the carbon injection rate, the resulting gasification rate was very high and it would be expected that the foam height would be the highest observed in this study. However, at very high injection rates the residual carbon loading in the slag will also be high, which could cause the antifoaming effect observed by Fruehan (1995). Therefore, the loss of foaming observed in this experiment is consistent with previous observations and with theories advanced in the current work.

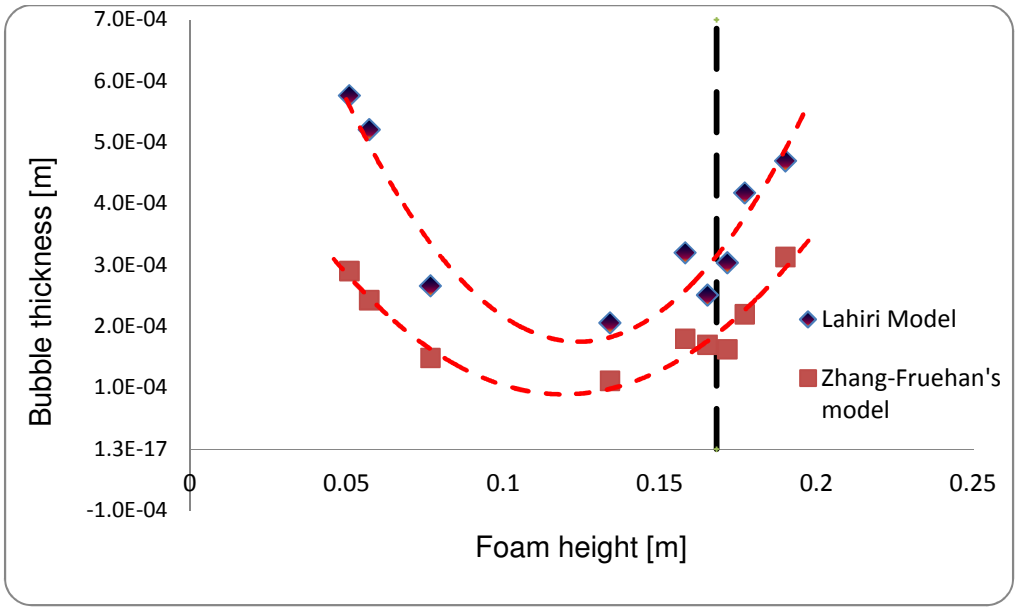

Figure 5. 2 Average bubble wall thickness vs. slag foam height

A plot of the average bubble size versus foam height is given in Figure 5.3

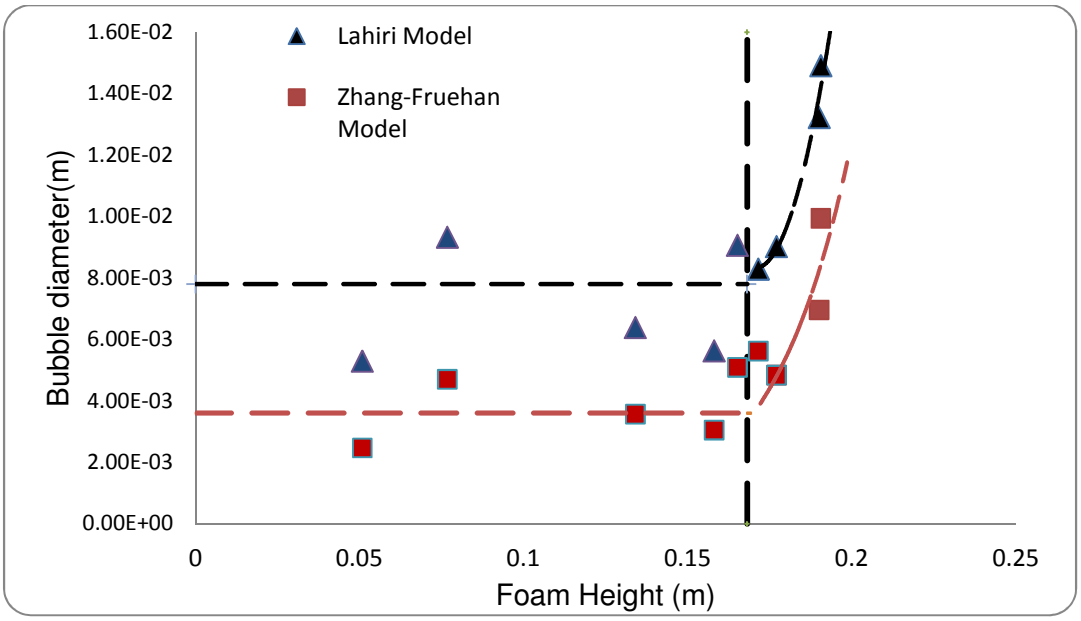

Figure 5. 3 Average bubble size vs slag foam height

According to the results of average bubble wall thickness and average bubble size, the assumption of $t_{cri} << d_{avg}$ may be not applicable because comparing results in Figure 5.2 and 5.3, the ratio of d_{avg} to t_{cri} is mostly less than 10; hence further improvement is required.

Void fraction is given by the ratio of measured foam height to the sum of measured foam height and consumed slag height. This concept is illustrated in Figure 5.4

$$\alpha \approx \frac{h_{foam}}{h_{foam} + h'_{slag}} \tag{5.6}$$

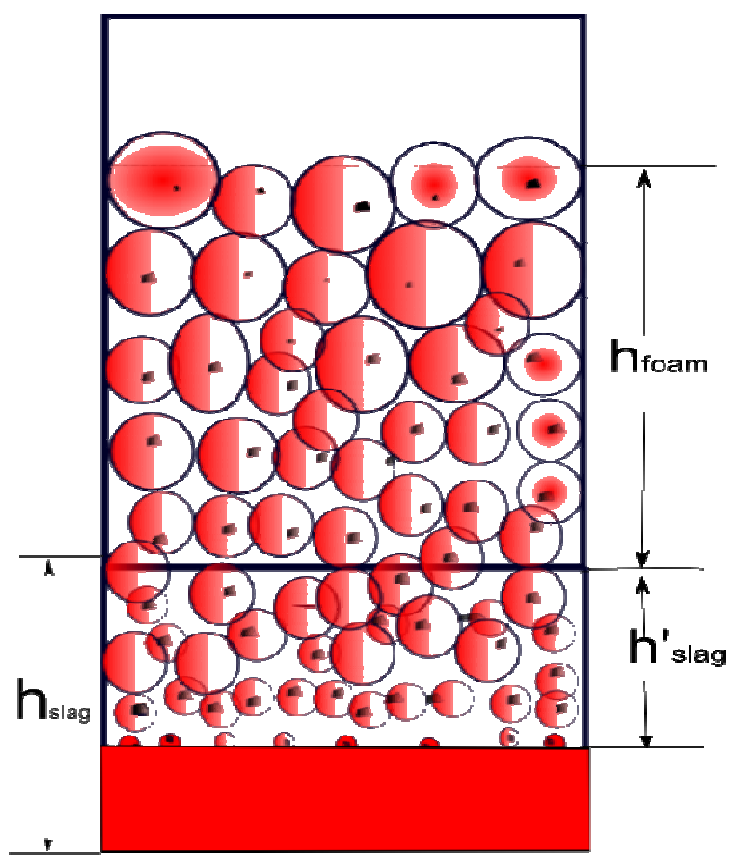

Figure 5. 4 Schematic of slag foaming with various foam void fraction

$$V_{slag} = \frac{\pi d_{cru}^{2}}{4} h_{slag}^{'} = \frac{1}{2} N_b \left(\frac{4\pi(\frac{d_{avg}}{2} + t_{cri})^3}{3} - \frac{4\pi(\frac{d_{avg}}{2})^3}{3} \right) \tag{5.7}$$

And

$$N_b = \frac{V_{gas}}{V_{bubble}} = \frac{\frac{\pi d_{cru}^{2}}{4} h_{foam}}{\frac{4\pi(\frac{d_{avg}}{2})^3}{3}} = \frac{3 h_{foam} d_{cru}^{2}}{2 d_{avg}^{3}} \tag{5.8}$$

Substituting equation 5.6 and 5.8 into equation 5.7 yields:

$$\frac{1-\alpha}{\alpha} = \frac{t_{cri}}{d_{avg}^{3}} (d_{avg}^{2} + 4 t_{cri}^{2} + 2 d_{avg} t_{cri}) \tag{5.9}$$

After the critical carbon injection rate, this equation can be modified to yield equation 5.10 by assuming that all unfoamed slag has been consumed for foaming.

$$\frac{h_{slag}}{h_{foam}} = \frac{t_{cri}}{d_{avg}^{3}} (d_{avg}^{2} + 4 t_{cri}^{2} + 2 d_{avg} t_{cri}) \tag{5.10}$$

where h'_{slag} is the unfoamed slag height consumed for foaming. Fruehan and et al. (1989) discussed void fraction α and suggested that slag foaming void fraction is between 0.7 and 0.9 for relatively low superficial gas velocity. Then bubble wall thickness can be calculated from equation 5.9 and 5.10 for foam void fraction α=0.7, 0.8, 0.9 and plotted in figure, 5.5, 5.6 and 5.7, respectively, versus foam height.

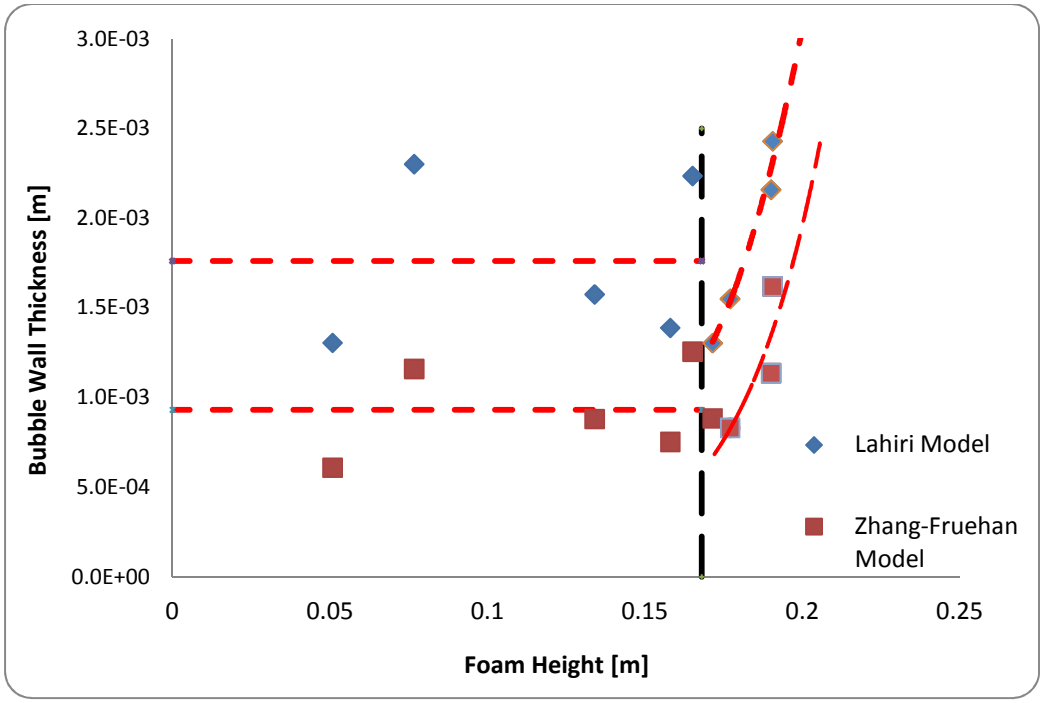

Figure 5. 5 Average bubble wall thickness vs. slag foam height at foam void fraction α=0.7 before critical point

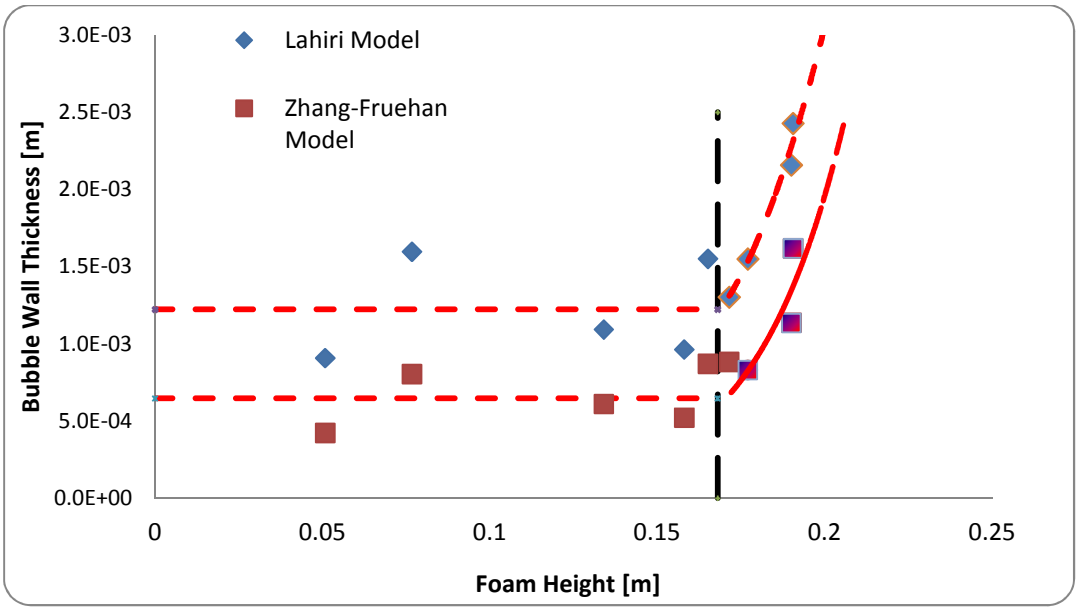

Figure 5. 6 Average bubble wall thickness vs. slag foam height at foam void fraction α=0.8 before critical point

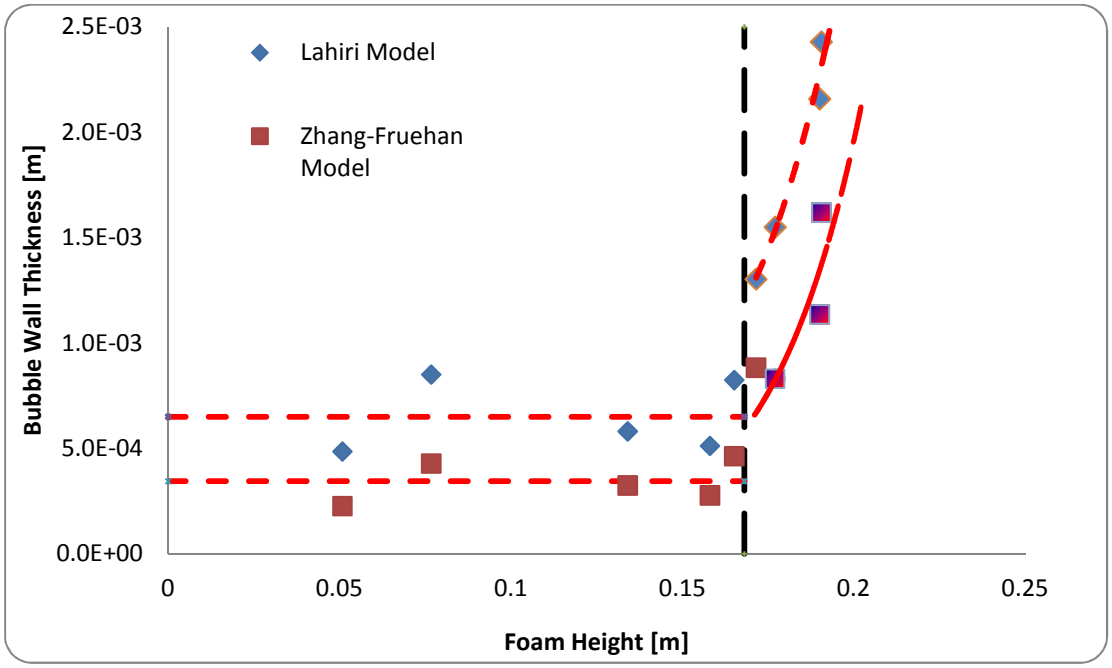

Figure 5. 7 Slag foam height vs. Average bubble wall thickness at foam void fraction α=0.9 before critical point

The average bubble diameter shown in Figure 5.3 and critical/average bubble wall thickness shown in figures 5.5, 5.6 and 5.7 are relative constant prior to the critical point (0.17 m from Fig. 4.4). Continued carbon injection beyond this point leads to an abrupt increase in average bubble size and rising bubble wall thickness. From these analyses, it can be concluded that bubbles maintain a relatively constant steady state size and wall thickness before the critical point. After the critical point, the foam can only grow if bubbles are stretched or fresh bubbles nucleate at the bubble walls. The data showing an increase in wall thickness as well as bubble size can only be correct if significant coalescence occurs. This results in larger bubbles which will have a greater tendency to rupture. It is not clear whether the decrease in the rate of foam growth is a consequence of accelerated rupture, or the greater difficulty of increasing bubble size compared with the formation of new bubbles from liquid, or a combination of both effects.

5.2 Average Bubble Diameter

Although Lahiri-Seetharaman (2002) and Zhang-Fruehan‘s (1995) foam index models were applied to predict average bubble size, these models were not widely validated for different slag compositions and temperatures. Meanwhile King (2009) developed a model to estimate instantaneous average bubble size, which used gas volume change inside

individual bubbles to predict bubble size. This model is based on one carbon particle attached to one bubble in the foam.

Average bubble size may be calculated from either equation 5.11, 5.12 or 5.13, from Lahiri and Seetharaman (2002), Zhang and Fruehan (1995) and King (2009) respectively.

$$d_{avg} = \frac{150\mu}{\rho\Sigma} \tag{5.11}$$

$$d_{avg} = \frac{115\mu^{1.2}}{\sigma^{0.2}\rho\Sigma} \tag{5.12}$$

$$d_{avg} = 1.24\left(\frac{M_{CO}}{\rho_{CO}}\right)^{\frac{1}{3}}\left(n_C^o - \frac{n_{C\_tot}}{N_P}\right)^{\frac{1}{3}} \tag{5.13}$$

Where Σ is the foam index in units of [s], σ is the slag surface tension in units of [Nm^{-1}], ρ is the slag density in units of [kgm^{-3}], μ is the slag viscosity in units of [Pa s], Mco is the molecular weight of CO [0.0280101 kg mol^{-1}], ρco is the density of CO [1.145 kg m^{-3}], Np is the number of carbon particles injected into slag, n^o_C is the initial amount of carbon in a carbon particle in units of [mol], and n_{c_tot} is the total amount of carbon remaining in a slag bubble at an instant time of t s.

Average bubble size can be evaluated directly from slag properties in foam index models, but this approximation cannot foresee the change of bubble size if the amount of carbon in slag is changed or the carbon injection rate is adjusted. King's model, on the other hand, described the whole process of changing bubble size while the total amount of carbon is increasing at the beginning and decreasing or stays constant after carbon injection ceases. According to King's work, most bubbles grow to a stable size in a very short time (less than 5 s), and then remain at steady-state. This may or may not show the real phenomenon in slag foaming because: there is no evidence to show whether or not each bubble attaches to a single carbon particle; some of the bubbles would burst when they reach an excessively large size; residual carbon particles on top of the slag change liquid physical properties; and fluid turbulence disturbs the pressure balance leading to bubble instability thus changing the liquid drainage rate.

The steady-state average bubble size calculated from King's model has relatively poor agreement with measurement, which is shown in Figure 2.7, compared to Lahiri-Seetharaman and Zhang-Fruehan's estimations. However, it should also be noted from Figure 4.1, which shows a large fraction of liquid slag in this sample, that whilst measured bubble size may be consistent with the predictions of Zhang and Fruehan (1995) and Lahiri and Seetharaman (2002), the observed void fraction is not. It is likely that the much lower void fraction observed in this frozen slags, is a result of bubble collapse on freezing. It may be that the agreement between prediction and measurement is entirely fortuitous and that the apparent disagreement in the work of King is caused by the

freezing process. However, it may also be that the bubbles that remain in the frozen slag are representative of those at high temperature and offer a reasonable estimate of average bubble size.

The results of King's average bubble size predictions appear to be overestimated. This means slag-gas interfacial area is greater in calculation than in the real case, but the prediction of carbon gasification rate and total amount carbon in the slag had good agreement with experimental measurement, which is shown in Figure 5.8.

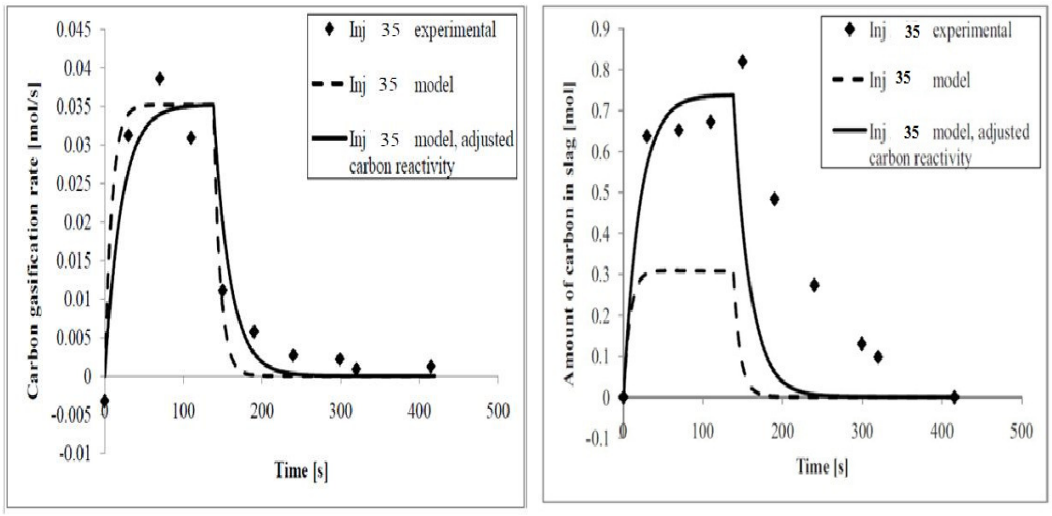

Figure 5. 8 Carbon gasification rate prediction & carbon in slag, experimental 35(King, 2009)

The analysis of these results suggests that King's model can predict reaction rate of injected carbon in slag very well, but needs further improvement for total interfacial area estimation as well as in predicting bubble size. The higher bubble size results may be explained by the fallacy that each carbon particle remains indefinitely within a bubble and

therefore continues to react and grow the bubble. The fact is that such carbon particles escape from ruptured bubbles. This carbon may still react with oxide from slag or CO_2, but has limited ability to generate bubbles on the top of the foam. Therefore, King's calculation may provide accurate results for total gas generated from carbon injection but not for bubble size.

It is reasonable to assume that foam keeps growing when carbon is injected in the first several seconds, then bubbles quickly grow to some saturated size or critical size. Further carbon injection leads to bubbles bursting and CO/CO_2 gas escapes from the foamed slag. This bubble rupture rate and gas generation rate are rapidly balanced which finally results in steady state slag foaming and a stable average bubble size. The average bubble size could be predicted from King's work if the initial time t is found. This is the time immediately before the first bubble bursts, or the maximum time for which slag traps an individual gas bubble without escaping.

The total gas generated from carbon injection is equal to the gas entrained in the slag foam plus the gas which has escaped from slag into the exhaust system at any time t. This can be expressed by Equation 5.14.

$$\frac{dn_{gas}}{dt} - \frac{dn_{gas-foam}}{dt} = \frac{dn_{gas\_out}}{dt} \qquad (5.14)$$

where n_{gas} is total amount of gas generated, n_{gas_foam} is the amount of gas in the foam, and n_{gas_out} is the amount of gas which has escaped from the foam.

When t< $t_{steady\text{-}state}$ or t at first bubble burst

$$\frac{dn_{gas}}{dt} \quad \frac{dn_{gas\_out}}{dt} \text{ or } \frac{dn_{gas\_out}}{dt} = 0 \qquad (5.15)$$

Accordingly

$$\frac{dn_{gas}}{dt} = \frac{dn_{gas-foam}}{dt} \qquad \text{or} \qquad n_{gas} = n_{gas-foam} \qquad (5.16)$$

Assuming the maximum foam height from experimental measurement is the steady-state foam height, the total volume of gas entrapped in the foam is represented in Equation 5.17.

$$V_{foam} = \pi(\frac{d_{cru}}{2})^2 h_{foam} \qquad (5.17)$$

Another important assumption is that the gas phase consists of only CO/CO_2 and all C in the gas is from injected carbon, then we have equation 5.18 and 5.19. This assumption is reasonable as carbon particles disperse in the slag at the injection point whereas carrier gas short circuits up the wall of the injection lance.

$$n_{gas\_foam} = n_{inj\_tot} - n_{c\_slag} \tag{5.18}$$

$$n_{gas\_foam} = \frac{V_{gas\_foam}}{\frac{T}{273} \times 22.414} \tag{5.19}$$

where n_{inj_tot} is total amount of carbon injected into the slag between time t_0 and t, and n_{c_slag} is the total amount of residual/non-reacted carbon in the slag at time t.

The steady state time t usually occurs several seconds after carbon injection starts hence t is much shorter than the period of carbon injection, and total amount of residual carbon could be calculated from equation 5.20 from King (2009).

$$n_{C\_slag} = n_C^{tot} = R_p n_c^{\ o} \left(\frac{1+\phi_{co}+p_{co_2}}{\Phi_1 \phi_{co}(p_{co_2}{}^{c} - p_{co_2})}\right)\left(1-\exp\left(-\frac{\Phi_1 \phi_{co}(p_{co_2} - p_{co_2}{}^{c})}{1+\phi_{co}-p_{co_2}} t\right)\right) \tag{5.20}$$

Equations 5.17, 5.18 and 5.19, may be combined with Equation 5.20 to calculate this steady state time t in Equation 5.21. This is then substituted into Equation 5.13 to approximate average bubble size.

$$0.349\frac{h_{foam}}{T} = tR_i - R_p n_c^{\,o}\left(\frac{1+\phi_{co}+p_{co_2}}{\Phi_1\phi_{co}(p_{co_2}{}^{c}-p_{co_2})}\right)\left(1-\exp\left(-\frac{\Phi_1\phi_{co}(p_{co_2}-p_{co_2}{}^{c})}{1+\phi_{co}-p_{co_2}}t\right)\right) \qquad (5.21)$$

where R_i is the carbon injection rate in units of [mol s^{-1}], R_p is the carbon injection rate in units of [particles s^{-1}], Φ_1 is the temperature-dependent carbon rate parameter [$atm^{-1}min^{-1}$], ϕ_{CO} is the temperature-dependent carbon rate parameter related to carbon surface adsorption by CO [atm], p_{CO2} is the equilibrium pressure [atm] of CO_2 in bubble surrounding the carbon, p^c_{CO2} is the pressure of CO_2 at the carbon-gas interface [atm]. $n°_C$ is the initial number of moles of carbon in a particle, h_{foam} is the measured foam height [m], T is the temperature in furnace [K], and t is the carbon particle residence time in the slag[s].

The results of this calculation of average bubble size are presented in Figure 5.9 together with previous predictions from King and experimental measurements. It shows excellent agreement with measured results. It should be noted that the present results also agree well with predictions of bubble size using models developed by Zhang and Fruehan (1995) and Lahiri and Seetharaman (2002). As was pointed out above, the measurement of bubble size in the current work may be considered questionable. However, the fundamental logic in the prediction with regard to a finite bubble life is an improvement on King (2009). In addition, no ex-situ bubble measurements or fitting parameters were used in developing the current model. As suggested above, it may be that quenching causes some bubble collapse but those that are captured offer a reasonable representation of the size distribution at high temperature. In any case, in the absence of reliable high

temperature measurements the current model appears to offer a reasonable method to estimate bubble size.

It is worth noting that the steady state time $t_{steady\text{-}state}$ employed in the current work is in the range of 2.25 to 3.75 s. The time to reach steady foaming is somewhat longer than the steady state time. However, these times do not represent the same physical phenomena. The steady state time for bubble life represents the lifetime of a single bubble under given (instantaneous) conditions: superficial gas velocity, temperature and slag properties. The time to achieve steady state foaming also includes the time to reach maximum gas generation rate, due to the accumulation of carbon in the slag. This latter time is considerably longer than the time it takes the foam to respond to a given set of conditions.

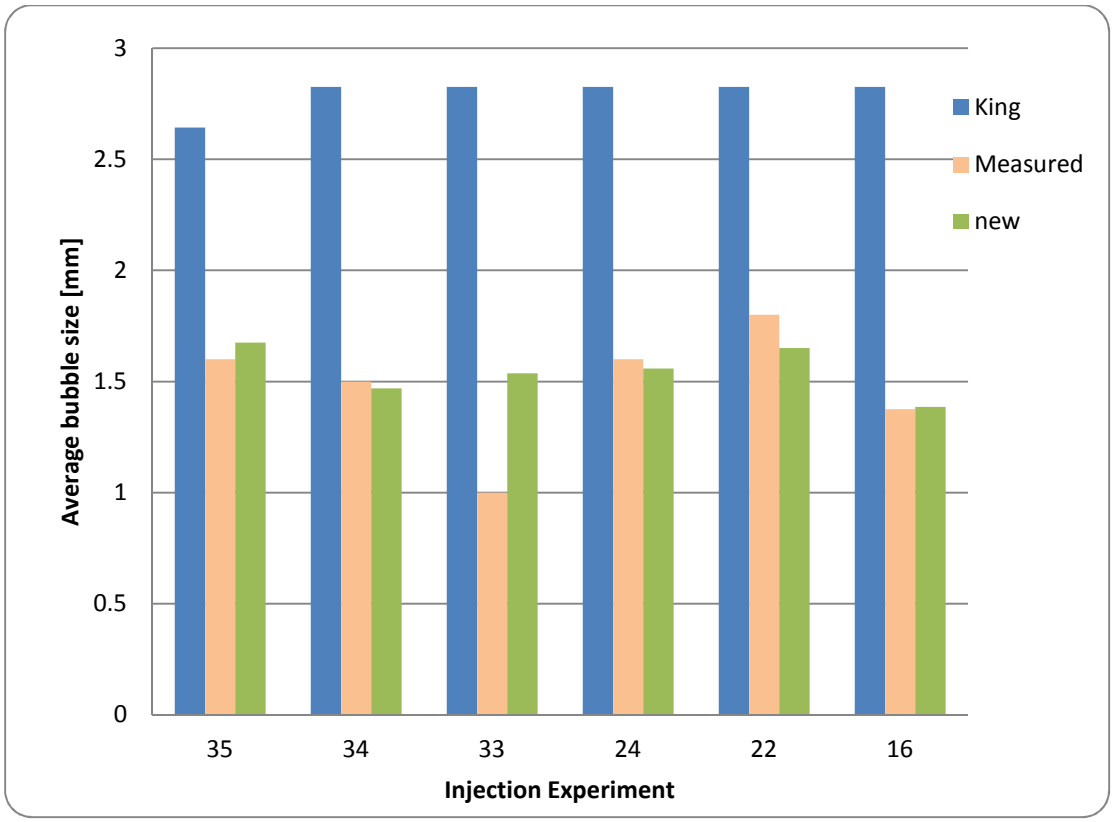

Figure 5. 9 Average bubble diameter prediction

Chapter 6: Conclusion

6.1 Conclusions

Coal injection into EAF slags has been extensively studied on a laboratory scale. Experimental results discussed in this research, in agreement with previous work from King (2009), show that an increase in slag foaming with carbon injection rate follows a linear relationship based on the foaming index, but at some critical foam height this relationship breaks down. The current work has shown that foaming is restricted by slag volume, and a critical carbon injection rate exists beyond which foaming is much less effective. This occurs when all residual liquid slag has been consumed in forming foam and is likely caused by either an increase in the energy required to grow bubbles beyond a certain size, by the increased tendency to rupture of bigger bubbles, or both. This may be exacerbated by large amounts of residual carbon particles increasing the tendency of bubbles to rupture.

Approximation of the bubble wall thickness from known slag properties and bubble size in the foam can be applied to identify a critical foam height and carbon injection rate as a function of slag volume and composition. Beyond the critical foam height it is clear that bubbles coalesce to form larger thicker walled bubbles; however, it is not clear whether

the foam grows by expansion of existing bubbles or the nucleation of fresh bubbles at the bubble walls.

A version of the model developed by King, is modified to consider the effect of bubbles bursting at the top of the foam. By estimating the lifetime of bubbles in the foam this offers an excellent the prediction of average bubble size in the foam.

6.2 Future Work

A kinetic model of the carbon-gas-slag system has been developed and applied to experimental results in this study and previous work. Modifications in this study, whilst greatly improving the predicted bubble size, have not yet been extended to predict reaction rate and therefore foam height. Future work will focus on extending this modification to prediction of kinetics.

The assumption states that one carbon particle only attaches to one bubble, whilst reasonable requires proof. An experiment will be designed in which X-ray photography is used to observe single or multiple carbon particles injected into EAF slag and foaming slag.

The carbon content at different levels within the foam is important information to elucidate the mechanism of bubble formation, growth rise through the foam and burst. Therefore, future work will measure carbon distribution with respect to position in the foam as a function of time and injection conditions.

A critical aspect in fully understanding the nature of foaming in response to carbon injection is the way in which carbon particles may contribute. A set of experiments will be conducted to analyze the effect of residual carbon on decreasing foam stability. This will be done by injecting types of carbon with different reactivities at the same injection rate; this will lead to the same steady state gasification rate but will yield different amounts of residual carbon. Therefore, the different foaming response can be attributed to the effect of carbon particles in the foam.

Understanding bubble escape is very important in predicting droplet swelling rates in BOF steelmaking. The current work will be extended to develop models to describe the escape of bubbles from swollen Fe-C-O droplets, which are essentially metal foams. The comparison of metal and slag systems will also be interesting from a fundamental perspective as the physical properties are quite different.

References

Barati, M., & Coley, K. (2005). *Metall. Mater. Trans. B , 36B*, 169-178.

Barati, M., & Coley, K. (2006). *Metall. Mater. Trans. B , 37B*, 61-69.

Brinkman, H. (1952). *J. Chem. Phys. , 20*, 571.

Cobrari, R., Atsuura, H., Halder, S., Walker, M., and Fruehan, R. (2009). *Metall. Mater. Trans. B ,* 40B, 940-948.

El-Rahaiby, R.J., Sasaki, Y., Gaskell, D., and Belton, G. (1986). *Metall. Mater. Trans. B ,17B*, 307-316.

Fruehan, R., Goldstein D., Sarma, B., Story S., Glaws, P., & Pasewicz, H. (2000). *Metall. Mater. Trans. B , 31B*, 891-898.

Gaskell, D. (2003). *Introduction to the Thermodynamics of Materials* (4th ed.). New York, NY: Taylor & Francis.

Ghag, S.S. , Hayes, P.C. and Lee H.G. (1998), *ISIJ International*, 38, 1201-1207.

Gregory, J. (1969), *Adv. Colloid Interface Sci.,* 2, 396-417.

Goel, R., & Kellogg, H. (1984). In H. Fine, & D. Gaskell (Ed.), *Proc. 2nd Int. Symp. on Metallurgical Slags and Fluxes* (pp. 347-355). Warrendale, PA: TMS-AIME.

Gou, H., Irons, G.A., and Lu, W.-K.(1996), *Metall. Mater. Trans., B, 27B*, 195-201

Guo, D. (1984). *Archiv Fur Das Eisenhuttenwesen , 55*, 183-188.

Iida, T., Sakai, H., Kita, Y., & Shigeno, K. (2000). *ISIJ International , 40*,

Supplement, S110-S114.

Ireland, P.M. (2009). *Chemical Engineering Science*, 64(23), 4866-4874.

Irons, G.A. (2005). *Howe Memorial Lecture, AISTech.* Charlotte, NC.

Irons, G.A. (2005, July). *AIST Trans.* , 111-123.

Ito, K., & Fruehan, R. (1989). *Metall. Trans. B , 20B*, 509-521.

Van der Schaaf, J. and Beerkens, R.G.C.(2006), *J. Colloid Interface Sci.,* 295, 218–229

Ji, F.-Z., Barati, M., Coley, K., & Irons, G. (2002). *60th Electric Arc Furnace Conference Proceedings, ISS*, (pp. 14-27). San Antonio, Texas.

Ji, F.-Z., Barati, M., Coley, K., & Irons, G. (2003). *ISS Tech 2003 Conference Proceedings*, (pp. 703-711). Indianapolis, IN.

Ji, F.-Z., Barati, M., Coley, K., & Irons, G. (2004). *VII International Conference on Molten Slags, Fluxes and Salts*, (pp. 399-405). South Africa.

Ji, F.-Z., Barati, M., Coley, K., & Irons, G. (2005). *CMQ , 44*, 85-94.

Ji, F.-Z., Coley, K., & Irons, G. (2005). *Conference of AIStech 2005 and ICS2005, ICS2005 Proceedings*, (pp. 423-430). Charlotte, NC.

Jiang, R., & Fruehan, R. (1991). *Metall. Mater. Trans. B , 22B*, 481-489.

Jung, S., & Fruehan, R. (2000). *ISIJ International , 40*, 348-355.

King, M. (2009). *M.A.Sc.. Thesis.* McMaster University, Hamilton, ON.

Kondratiev, A., & Jak, E. (2001). *Metall. Mater. Trans. B , 32B*, 1015-1025.

Kondratiev, A., & Jak, E. (2005). *Metall. Mater. Trans. B , 36B*, 623-638.

Larson,H.L. and Chapman, J.(1953), *Trans. AIME*,1089-1096.

Lahiri, A., & Seetharaman, S. (2002). *Metall. Mater. Trans. B , 33B*, 499-502.

Li, Y., & Ratchev, I. (2002). *Metall. Mater. Trans. B , 33B*, 651-660.

Li, Y., Ratchev, I., Lucas, J., Evans, G., & Belton, G. (2000). *Metall. Mater. Trans. B , 31B*, 1049-1057.

Lotun, D., & Pilon, L. (2005). *ISIJ International , 45*, 835-840.

Matsuura, H., Ishida, I., & Tsukihashi, F. (2004). *ISIJ International , 44*, 1494-1500.

Matsuura H. & Fruehan R. (2009), ISIJ International, 49, 1530–1535

Mills, K., & Keene, B. (1987). *Int. Mater. Rev. , 32*, 1-120.

Min, D., Han, J., & Chung, W. (1999). *Metall. Mater. Trans. B , 30B*, 215-221.

Morales, R., Lule, R., Lopez, F., Camacho, J., & Romero, J. (1995). *ISIJ International, 35*, 1054-1062.

Morales, R., Rodriguez, H., & Conejo, A. (2001). *ISIJ International , 41*, 426-435.

Morales, R., Rodriguez, H., Vargas-Zamora A & Conejo, A. (2002). *Ironmaking and Steelmaking, 29*, 445-453

Morales, R., Rodriguez, H., Garnica, P., & Romero, A. (1997). *ISIJ International, 37*, 1072-1080.

Mori, M., Morita, K., & Sano, N. (1996). *ISIJ International, 36*, 624-630.

Nakamoto M., Toshihiro T., Lauri H. and Marko H.(2007), *ISIJ International ,* 47, 211-216

Ogawa, Y., Huin, D., Gaye, H., & Tokumitsu, N. (1993). *ISIJ International, 33*, 224-232.

Olivares R.,Brungs M.P., and Lian H.(1991), *Metall. Mater. Trans. B* , 22B,305-307.

Ozturk, B., & Fruehan, R. (1995). *Metall. Mater. Trans. B , 26B*, 1086-1088.

Pilon, L., & Viskanta, R. (2004). *Chem. Eng. Process. , 43*, 149-160.

Rodriguez, H., Conejo, A., & Morales, R. (2001). *Steel Res. , 72*, 298-303.

Sarma, B., Cramb, A., & Fruehan, R. (1996). *Metall. Mater. Trans. B , 27B*, 717-730.

Skupien & Gaskell D.R. (2000), *Metall. Mater. Trans. B, 31B,* 921-925.

Story, S., & Fruehan, R. (2000). *Metall. Mater. Trans. B , 31B*, 43-54.

Story, S., Sarma, B., Fruehan, R., Cramb, A., & Belton, G. (1998). *Metall. Mater. Trans. B , 29B*, 929-932.

Morales ,R.D., Conejo, A.N. , and Rodriguez, H.H. *Metall. Mater.Trans. B. 33B,* 187-199.

Thiele, E. (1939). *Ind. Eng. Chem., 31*, 916-920.

Tien, R., & Turkdogan, E. (1970). *Carbon, 8*, 607-621.

M. Timuchin, M. and Morris, A.E.(1970), *Metall. Trans.B*, 1B,3193-3201.

Tran, S., Sun, S.,Jahanshahi, S.(1997), *V Int. Conf. on Molten slags, fluxes and salts*, Sydney, Australia.115-123

Turkdogan, E., & Vinters, J. (1969). *Carbon, 7*, 101-117.

Turkdogan, E., & Vinters, J. (1970). *Carbon, 8*, 39-53.

Turkdogan, E., Koump, V., Vinters, J., & Perzak, T. (1968). *Carbon, 6*, 467-484.

Urbain, G. (1987). *Steel Res., 58*, 111-115.

Turkdogan, E. Olsson, R. G., and Vinters, J. (1970), *Carbon*, 8,545–64.

Urbain, G., Cambier, F., Deletter, M., & Anseau, M. (1981). *Trans. J. Br. Ceram.*

Soc. , 80, 139-141.

Visser, J. (1972), *Adv. in Colloid and Interface Sci*., Volume 3, Issue 4.331-363

Vrij, A. (1966), *Discuss. Faraday Soc.* 42, 23-33.

Warczok, A., & Utigard, T. (2000). *Steel Res., 71*, 277-280.

Wu, L.S., Albertsson, G.J. and Du, S. (2010), *Ironmaking and Steelmaking*, 37,612-619

Zhang, L., & Jahanshahi, S. (1998). *Metall. Mater. Trans. B, 29B*, 177-195.

Zhang, Y. & Fruehan .R. (1995). Metall. *Mater. Trans. B, 26B*, 803-812.

Zhu, M-Y & Du S.(2000) ,Process Metallurgy, Steel Research, 71, 76–82.

Zhu, T-X., Coley, K.S., Irons, G.A. and Ray, S.(2011), *Proceedings of AISTech*, Indianapolis, May 2011.

Appendix

A.1 Calculation of Maximum Gasification Rate

A.1.1 Slag Composition

Slag samples were collected directly from experiments at different depths and time during carbon injection, then quenched into cold water and dried in an oven for 12 hours before ICP analysis. The results from ICP analysis include: SiO_2, P_2O_5, Al_2O_3, CaO, MgO, MnO, and FeO/Fe_2O_3. The average values of composition which were obtained from various depths and time in each experiment were used to determine slag properties; for instance, calculating slag viscosity, surface tension and density. ICP analysis results only provided the total iron content in a sample thus the Fe^{2+}/Fe^{3+} ratio was estimated from Guo (1984). The ratio of Fe_2O_3/FeO is described as follows:

$$\frac{Fe_2O_3(wt\%)}{Fe\ O\ (wt\%)} = A + \sum B_i(X_i(wt\%)) \qquad \text{(a.1)}$$

then

$$A = \frac{(0.8541 + \frac{296.7}{T}) - 1}{3 - 2(0.8541 + \frac{296.7}{T})} \times \frac{159.69}{71.84} \qquad \text{(a.2)}$$

Table A. 1 Bi values for different slag components (Guo, 1984)

Component	**Bi**
CaO	**0.0073**
MgO	**0.0066**
MnO	**0.001**
SiO_2	**-0.007**
P_2O_5	**-0.0074**

Therefore, A and B values were calculated from equation a.2 and table A.1, X_i is wt% of each component analyzed from ICP.

A.1.2 Calculation of Equilibrium CO_2/CO at the Slag-Gas Interface and Carbon-Gas Interface

Ji and et al. (2002, 2003, 2004 and 2005) conducted in-depth research on carbon-gas-slag kinetics which have been discussed in Chapter 2 of this thesis.

The carbon-gas interface reaction was assumed to be ideal carbon reacting with CO_2 to produce CO and can be expressed as below:

$C(s) + CO_2(g) = 2CO(g)$ (a.3)

thus

$$\ln K = 20.983 - \frac{20530.56}{T}$$ (a.4 Gaskell, 2003)

Total pressure of CO and CO_2 was assumed to be 1 atm hence the equilibrium pressures of CO_2/CO are only dependent upon temperature T [K], and then P^C_{CO2} and P^C_{CO} can be solved in equation a.5

$$\frac{(1-P^C_{CO_2})^2}{P^C_{CO_2}} = \exp(20.983 - \frac{20530.56}{T})$$ (a.5)

The calculation of equilibrium pressure of CO_2/CO at the slag-gas interface was discussed by Goel and Kellogg (1984) and was applied in King (2009). However, the applicable temperature would be much lower than that of the current carbon injection experiments. Furthermore, by combining work from Mori et al.(1996), Tran and Jahanshahi (1997), Larson & Chapman (1953), Timuchin & Morris (1970), Li & Ratchev (2002), and Matsuura et al. (2004), Ji and et al. (2005) developed a relationship between Pco_2/Pco and $Fe^{2+/}Fe^{3+}$ this is represented in equation a.6.

$$\log(\frac{P^S_{CO_2}}{P^S_{CO}}) = 0.912 + 2.421\log(\frac{Fe^{3+}}{Fe^{2+}}) - 0.504B + 0.274(\frac{10^4}{T}) \quad \text{(a.6)}$$

Where

$$B = \frac{wt\%CaO}{wt\%SiO_2} \quad \text{(a.7)}$$

where P^s_{CO2} is the equilibrium partial pressure of CO_2 at the slag-gas interface in units of [atm], P^s_{CO} is equilibrium partial pressure of CO at slag-gas interface in units of [atm], B is basicity of slag in ratio of CaO to SiO_2, T is slag temperature [K], and Fe^{3+}/Fe^{2+} ratio could be calculated from Guo's model (1984).

A.1.3 Off-gas Analysis and Results

Gas samples were analyzed by Gas Chromatography to determine instantaneous carbon gasification rate by mass balance calculation. This calculation assumes all carbon injected into slag reacts to form CO and CO_2 in the off-gas system. The data obtained by Gas Chromatography are %CO, %CO_2, %N_2, %H_2, %O_2. Ji and et al. (2002, 2003, 2004 and 2005) developed a method to calculate post-combustion in carbon injection into EAF slags, and simplified post-combustion reaction as following:

$$CO + 0.5O_2 = CO_2 \quad \text{(a.8)}$$

Neglecting H_2 to simplify calculation, because $\%H_2$ is a relatively small fraction of the overall gas composition.

Since equilibrium gas pressure at the slag-gas interface and carbon-gas interface are not in equilibrium, the actual CO_2 pressure in the gas phase would be closer to that in equilibrium with faster reacting interface and the exact value can be expressed by equation a.9.

$$p_{CO_2}^{\chi} = \chi p_{CO_2}^{S} + (1-\chi) p_{CO_2}^{C} \quad \text{(a.9)}$$

The parameter has a value between 0 and 1, and is determined as the value which closes the mass balance for a given experiment. The error introduced by this approach may be significant when gas generation rate is low and therefore air entrainment is also significant. However, during and shortly after injection, when gas generation rates are high, it is not important to account for the very small amount of entrained air. Therefore, although this approach may introduce error it is not significant during the part of the process with which we are most concerned.

Ji, et al. developed a method to calculate carbon gasification rate from off gas composition. The mathematical equations are shown below:

$$Q_c = \frac{0.21 Q_{N_2}(1 - O_2^{'} - N_2^{'}) + Q_{N_2}(0.79 O_2^{'} - 0.21 N_2^{'})}{0.21 N_2} \quad \text{(a.10)}$$

And

$$\%CO_2^{\chi} = 100\, p_{CO2}^{\chi} = 100[\chi\, p_{CO2}^{S} + (1-\chi)\, p_{CO2}^{C}] \quad \text{(a.11)}$$

$$\Delta\%CO2 = \%CO_2 - \%CO_2^{\chi} \quad \text{(a.12)}$$

$$O_2^{'} = \frac{\%O_2 + 0.5\Delta\%CO_2}{\%CO + 1.5\Delta\%CO_2 + \%O_2 + \%N_2 + \%CO_2^{\chi} + \%H_2} \quad \text{(a.13)}$$

$$N_2^{'} = \frac{\%N_2}{\%CO + 1.5\Delta\%CO_2 + \%O_2 + \%N_2 + \%CO_2^{\chi} + \%H_2} \quad \text{(a.14)}$$

$$CO^{'} = \frac{\%CO + \Delta\%CO_2}{\%CO + 1.5\Delta\%CO_2 + \%O_2 + \%N_2 + \%CO_2^{\chi} + \%H_2} \quad \text{(a.15)}$$

$$CO_2^{'} = \frac{\%CO_2^{\chi}}{\%CO + 1.5\Delta\%CO_2 + \%O_2 + \%N_2 + \%CO_2^{\chi} + \%H_2} \quad \text{(a.16)}$$

$$H_2^{'} = \frac{\%H_2}{\%CO + 1.5\Delta\%CO_2 + \%O_2 + \%N_2 + \%CO_2^{\chi} + \%H_2} \qquad \text{(a.17)}$$

Therefore combined equations a.11, a.12, a.13, a.14, a.15, a.16, a.17, and modified equation a.10, final expression for gasification of carbon can be expressed as equation a.18.

$$Q_C = -Q_{H_2} + \frac{0.21Q_{N_2}(\%CO + \%CO_2 + \%H_2)}{0.21\%N_2 - 0.79\%O_2 - 0.395\%CO_2 + 39.5[\chi p_{CO_2}^{S} + (1-\chi)p_{CO_2}^{C}]} \qquad \text{(a.18)}$$

where Q_{H2} is hydrogen flow rate from volatiles in injected coal, in unit of [mol s^{-1}], Q_{N2} is nitrogen flow rate from both carrier gas and air, in unit of [mol s^{-1}], parameter χ was evaluated from carbon balance when summation of carbon gasified in different time intervals is equal to total amount of carbon injected into the slag. This process is described by eqn. a.19. Then maximum experimental carbon gasification rate was found by comparing with different time interval results in each experiment.

$$\sum_{i=1}^{n} \Delta t_i Q_{C_i} = n_C^{inj} \qquad \text{(a.19)}$$

A.2 Experimental

The experimental data used in calculations of the type described above are presented below to allow the reader to recalculate data presented in this thesis. It should be noted that conditions inside the gas stream are at steady state with respect to injection rate and carbon reaction with slag. The reader is cautioned against making assumptions about gas phase equilibrium and the value of the data in determining equilibrium constants.

Table A. 2 Measured slag compositions after applying model by Guo (1984)

Wt%	**36**	**37**	**38**	**39**
SiO_2	23.65	20.35	22.05	23.62
P_2O_5	0.14	0.06	0.06	0.06
Al_2O_3	5.69	4.95	5.23	5.13
CaO	37.87	34.86	36.53	36.05
MgO	8.40	6.50	7.86	7.88
MnO	2.27	1.10	0.97	1.09
Fe_2O_3	3.53	8.02	4.13	3.80
FeO	18.45	21.10	23.16	22.38

Table A. 3 Experiment 36 measured gas composition

Time [s]	%CO_2	%O_2	%N_2	%CO	%H_2
0	3.53	11.56	84.81	0.10	0.00
34	8.36	0.48	15.50	70.00	5.66
77	5.99	0.94	16.41	70.04	6.61
113	6.59	2.40	17.10	66.39	7.53
164	16.40	6.23	59.77	17.06	0.53

Table A. 4 Flow rate of N_2 and H_2 and gasification rate of carbon for experiment 36

Time [s]	Q_{N2}[mol s^{-1}]	Q_{H2}[mol s^{-1}]	Q_C[mol s^{-1}]
0	0.00582	0.00236	-0.00174
34	0.00582	0.00236	-0.23185
77	0.00582	0.00236	0.32530
113	0.00582	0.00236	-0.10803
164	0.00561	0.00000	0.03566
234	0.00561	0.00000	0.00421
282	0.00561	0.00000	0.00223
365	0.00561	0.00000	0.00271
421	0.00561	0.00000	0.00226
494	0.00561	0.00000	0.00774
542	0.00561	0.00000	0.00370
663	0.00561	0.00000	0.00225

Table A. 5 Experiment 37 measured gas composition

Time [s]	%CO_2	%O_2	%N_2	%CO	%H_2
0	0.00	15.91	84.09	0.00	0.00
32	11.03	0.00	25.15	54.26	9.56
49	10.00	0.30	21.71	59.18	8.81
81	8.13	0.00	33.86	45.10	12.90
100	8.65	0.00	37.93	39.46	13.96
172	9.93	0.86	60.61	26.47	2.12

Table A. 6 Flow rate of N_2 and H_2 and gasification rate of carbon for experiment 37

Time [s]	Q_{N2}[mol s^{-1}]	Q_{H2}[mol s^{-1}]	Q_C[mol s^{-1}]
0	0.0061589	0.002356	-0.00236
32	0.0061589	0.002356	0.075144
49	0.0061589	0.002356	0.142098
81	0.0061589	0.002356	0.017902
100	0.0059487	0.002356	0.013544
172	0.0059487	0	0.005696
229	0.0059487	0	0.005831
285	0.0059487	0	0.005797
369	0.0059487	0	0.004015
422	0.0059487	0	0.01256
484	0.0059487	0	0.00526
543	0.0059487	0	0.003126
663	0.0059487	0	0.002194

Table A. 7 Experiment 38 measured gas composition

Time [s]	%CO_2	%O_2	%N_2	%CO	%H_2
0	5.53	8.73	85.74	0.00	0.00
33	11.25	1.56	21.38	59.64	6.17
50	8.21	0.00	11.24	73.67	6.88
98	9.01	0.00	8.71	76.01	6.27
168	10.37	0.00	27.25	60.44	1.94

Table A. 8 Flow rate of N_2 and H_2 and gasification rate of carbon for experiment 38

Time [s]	Q_{N2}[mol s^{-1}]	Q_{H2}[mol s^{-1}]	Q_C[mol s^{-1}]
0	0.0060521	0.002826	-0.00226
33	0.0060521	0.002826	0.039944
50	0.0060521	0.002826	0.040657
98	0.0060521	0.002826	0.063528
168	0.0057999	0.002826	0.014536
223	0.0057999	0	0.006217
263	0.0057999	0	0.004385
337	0.0057999	0	0.0036
382	0.0057999	0	0.006776
422	0.0057999	0	0.002951
472	0.0057999	0	0.002296
541	0.0057999	0	0.002903
661	0.0057999	0	0.001801

Table A. 9 Experiment 39 measured gas composition

Time [s]	%CO_2	%O_2	%N_2	%CO	%H_2
0	5.20	7.18	87.02	0.00	0.00
33	10.89	1.13	17.58	63.21	7.20
50	9.59	0.00	11.34	72.16	6.91
95	9.02	0.27	20.90	60.59	9.22
162	7.73	0.00	30.32	59.57	2.38

Table A. 10 Flow rate of N_2 and H_2 and gasification rate of carbon for experiment 39

Time [s]	**Q_{N2}[mol s^{-1}]**	**Q_{H2}[mol s^{-1}]**	**Q_C[mol s^{-1}]**
0	0.0060521	0.002826	-0.00234
33	0.0060521	0.002826	0.06839
50	0.0060521	0.002826	0.07007
95	0.0060521	0.002826	0.025261
162	0.0057999	0.002826	0.01071
221	0.0057999	0	0.004766
282	0.0057999	0	0.004353
374	0.0057999	0	0.003191
421	0.0057999	0	0.002353
479	0.0057999	0	0.001847
543	0.0057999	0	0.002867
661	0.0057999	0	0.001624